

THESIS

INHIBITION OF A TRUNCATED FORM OF HUMAN MITOCHONDRIAL KIDNEY-TYPE
GLUTAMINASE (HKGA₁₂₄₋₅₅₁) BY BIS-2-(5-PHENYLACTAMIDO-1,2,4-THIALDIAZOL-
2-YL)ETHYL SULFIDE (BPTES)

Submitted by

Erik William Hartwick

Department of Biochemistry and Molecular Biology

In partial fulfillment of the requirements

For the Degree of Master's of Science

Colorado State University

Fort Collins, Colorado

Summer 2011

Master's Committee:

Advisor: Norman Curthoys

P. Shing Ho
Olve Peersen
Donald Mykles

Copyright by Erik William Hartwick 2011

All Rights Reserved

ABSTRACT

INHIBITION OF A TRUNCATED FORM OF HUMAN MITOCHONDRIAL KIDNEY-TYPE GLUTAMINASE (hKGA₁₂₄₋₅₅₁) BY BIS-2-(5-PHENYLACTAMIDO-1,2,4-THIADIAZOL-2-YL)ETHYL SULFIDE (BPTES)

Mitochondrial glutaminase (GA) catalyzes the hydrolysis of glutamine producing glutamate and an ammonium ion. There are three isoforms of mammalian GA that are essential to hepatic ureagenesis, renal ammoniogenesis, synthesis of the neurotransmitter glutamate, and the catabolism of glutamine. Here we focus on the human KGA isoform that is predominantly expressed in kidney, brain, intestine, and tissues of the immune system. Recent publications suggest that GA is a novel target for developing new cancer therapeutics. These studies have indicated that inhibition of GA by small molecule inhibitors significantly reduces the size of tumors in rats and inhibits growth of transformed cells in culture. A truncated form of human KGA (hKGA₁₂₄₋₅₅₁) that contains amino acids 124-551, was produced to delete the C-terminal sequences that are unique to the KGA and GAC isoforms. This construct was assayed in the presence of (bis-2-(5-phenylactamido-1,2,4-thiadiazol-2-yl)ethyl sulfide (BPTES). BPTES is a potent small molecule inhibitor of mammalian GA that was previously shown to inhibit rat KGA in μM concentrations. In the current study, we adapted the standard GA assay to a microtiter plate format and used it to characterize the inhibition of hKGA₁₂₄₋₅₅₁ using μM amounts of BPTES.

Our data indicate that BPTES is a mixed non-competitive inhibitor at low concentrations of phosphate, but at higher phosphate concentrations the inhibition is predominantly uncompetitive. Lastly, gel filtration and dynamic light scattering experiments were performed to determine if hKGA₁₂₄₋₅₅₁ oligomers are formed in the presence of BPTES and to characterize the effect of increasing concentrations of phosphate. The data suggest that in the absence or presence of phosphate and in the absence of BPTES, the hKGA₁₂₄₋₅₅₁ exists as a dimer, but in the presence of BPTES the molecular weight shifts to a tetramer or higher oligomer. The combined data indicate that BPTES is a potent lead compound for the development of a therapeutic inhibitor of human GA that may be a potential cancer therapeutic.

TABLE OF CONTENTS

Introduction.....	1
Materials and Methods.....	7
Results.....	14
Discussion.....	35
References.....	45
Appendix 1.....	48

Introduction

Mitochondrial glutaminase (GA) catalyzes the hydrolysis of glutamine producing glutamate and ammonium ion (1). GA is localized to the mitochondrial matrix. It contains an amphipathic α -helix encoded within exon 1 that is required to target GA to the mitochondrion (2). GA is essential to hepatic ureagenesis (1), renal ammoniagenesis (3, 4), synthesis of the neurotransmitter glutamate (5-7), and the catabolism of glutamine as an energy source (1, 8-10).

There are three isoforms of mammalian GA encoded by two separate genes (11, 12). The liver type glutaminase (LGA) is encoded by 18 exons on chromosome 12. The kidney type glutaminase (KGA) gene spans 82 kb on chromosome 2 and encodes 19 exons. KGA lacks sequence encoded by exon 15, but does include sequence from exons 1-14 and 16-19. The glutaminase variant (GAC) is an alternatively spliced isoform of the kidney type glutaminase. GAC contains sequence encoded by exons 1-15 and is predominantly expressed in the heart, pancreas, placenta, and lungs. The KGA isoform is predominantly expressed in kidney, brain, intestine, and tissues of the immune system (11). Comparison of three GA isoforms shows that human hLGA and hKGA have distinct N terminal sequences (Figure 1). All three isoforms have different C-termini; however, all isoforms share a common highly conserved core sequence (13). This core sequence is also similar to the bacterial glutaminase suggesting that the core sequence, located in the middle, contains the catalytic domain or active site of GA (13).

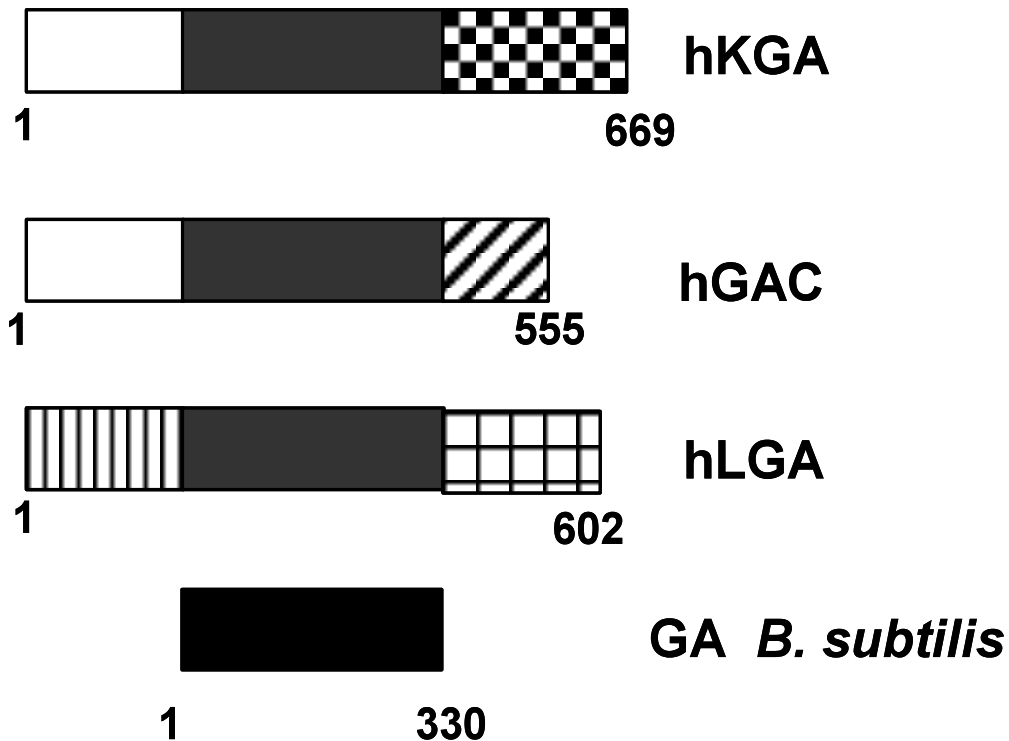


Figure 1 Comparison of human glutaminase isoforms and bacterial glutaminase

The three human glutaminase isoforms, kidney type glutaminase (hKGA), the kidney type glutaminase variant (hGAC), and the liver type glutaminase (hLGA), are compared to the bacterial glutaminase. There is a common core in the middle of the enzyme that is highly conserved in each glutaminase isoform that is represented by the black bar. hKGA and hGAC isoforms share an identical N-terminus, which differs from the hLGA isoform. Each of the human glutaminase isoforms has a distinct C-terminal region.

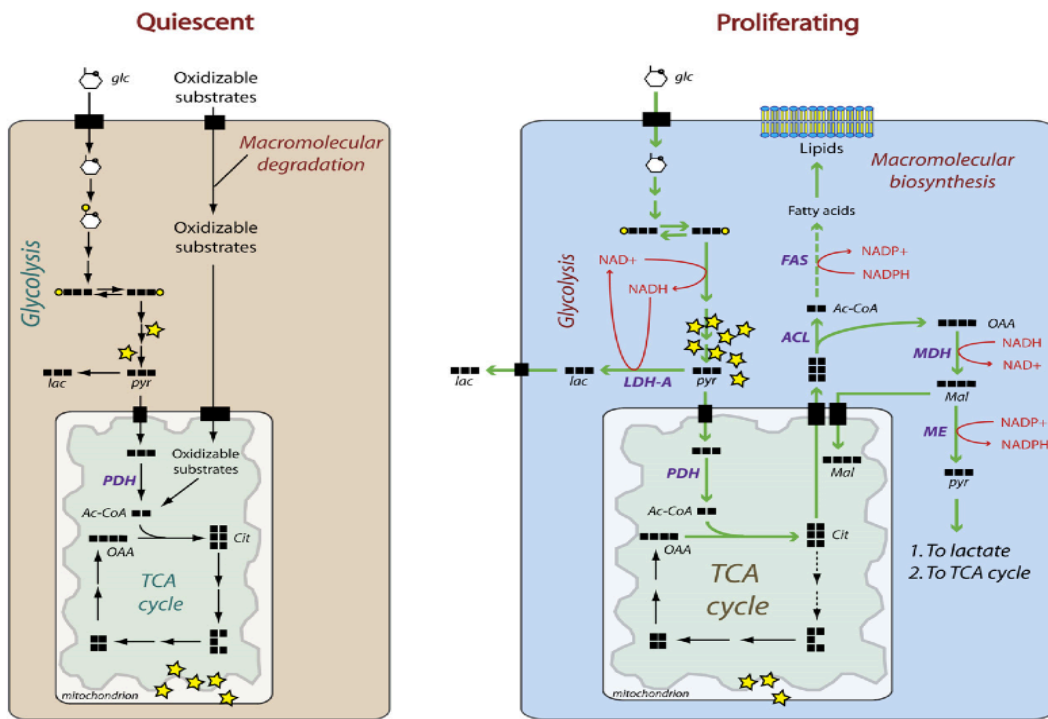
The catabolism of glutamine plays a central role in cellular metabolism.

Glutamine catabolism is involved in ureagenesis in hepatic tissue and is strongly activated in renal tissue during onset of metabolic acidosis (1, 3, 4). The conversion of glutamine to glutamate by GA followed by subsequent deamination by glutamate dehydrogenase leads to the formation of α -ketoglutarate (1). The further catabolism of α -ketoglutarate in the TCA cycle produces the high-energy electron carrier molecules, reduced nicotinamide adenine dinucleotide (NADH) and flavin adenine dinucleotide (FADH), for oxidative phosphorylation and can lead to the production of glucose through gluconeogenesis (1). α -Ketoglutarate can also be used to produce the amino acids aspartic acid and asparagine by transamination of oxaloacetate and a subsequent amidotransferase reaction, respectively. The formation of glutamate by either a transamination reaction or the glutaminase reaction can lead to the production of the amino acids proline and arginine as well as other metabolites central to the formation of urea such as ornithine and citrulline.

Since glutamine plays such a vast role in cellular metabolism and the production of high-energy molecules it has been suggested that glutamine is an essential fuel for rapidly dividing tissues and cancer cells (8, 14, 15). Recent studies have indicated that the metabolism of glutamine is just as important as the metabolism of glucose in cancer cells and transformed cell cultures (8, 15). It has been long established that the transport and metabolism of glucose leading to the formation of lactic acid is significantly increased in cancer cells, as explained by the Warburg effect (9, 16, 17). The Warburg effect suggests that the catabolism of glucose is increased significantly, but is largely utilized for the production of lactic acid even under

aerobic conditions (9) (Figure 2). The increased production of lactic acid is inefficient when compared to the ATP production through oxidative phosphorylation. However, recent publications suggest that the uptake of glutamine is also significantly increased, indicating that glucose catabolism is not the only, or even the main source of energy for cancer cells and transformed cells (8, 16, 18) (Figure 3). New studies indicate that inhibition of mitochondrial kidney-type glutaminase by siRNA knock-down and small molecule inhibitors can reduce the growth and size of tumors in rats and transformed cell culture (15, 19). This recent data suggests that GA is a target for developing novel cancer therapeutics.

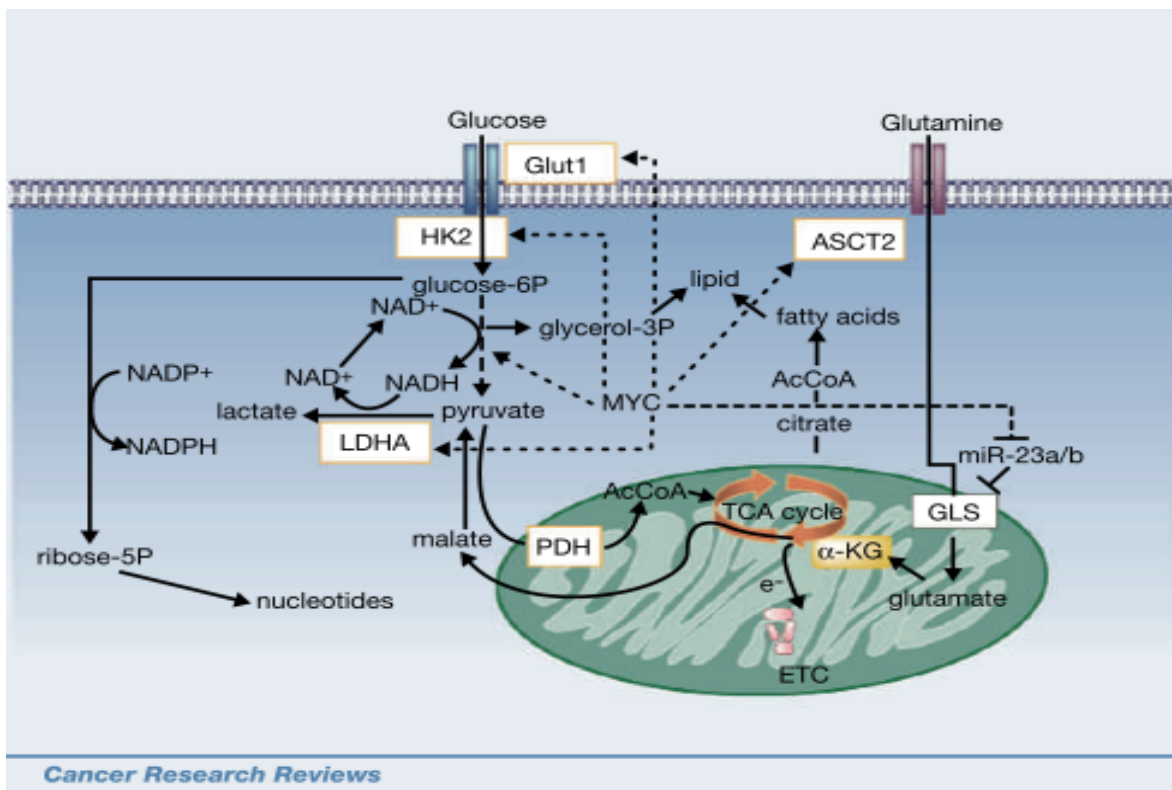
Furthermore, current studies suggest Rho family GTPases and the Dbl protein family are involved not only in transformation of cells, but are also responsible for the increased glutamine catabolism by activating GA (8). Rho family GTPases act as a super regulator, or switch, that mediates signal transduction from the plasma membrane to alter cell polarity, gene transcription, cell cycle progression and regulation, microtubule dynamics, vesicle transport, and enzymatic activities (20). Small GTPases are regulated in part by the binding and hydrolysis of GTP. Guanine nucleotide exchange factors (GEFs) aid in the binding of GTP activating small GTPases like the Rho family. GTPase activating proteins (GAPs) aid in the hydrolysis of GTP resulting in inorganic phosphate and GDP bound, inactive GTPase. GTPases can also be regulated by guanine nucleotide exchange factor inhibitors (GDIs), which bind C-terminal post-translational modifications (e.g. prenylation) of small



DeBerardinis, R. J., Lum, J. J., Hatzivassiliou, G., and Thompson, C. B. (2008) The biology of cancer: metabolic reprogramming fuels cell growth and proliferation, *Cell Metab* 7, 11-20.

Figure 2. The Warburg Effect

The metabolic flux between a quiescent cell (left panel) and a proliferating cell (right panel) as described by the Warburg effect. During a quiescent cell state glucose is catabolized through the glycolytic pathway and fully oxidized in the TCA cycle. This produces the needed electron carriers for oxidative phosphorylation producing large quantities of ATP (stars). During a proliferating cellular state the metabolic flux changes significantly under aerobic conditions. Larger quantities of glucose are consumed; however, glucose is not fully oxidized through the TCA cycle generating the needed ATP. Majority of the glucose is catabolized leading to the formation of lactic acid. As indicated by the diagram, most of the ATP generated is through the glycolytic pathway only forming small quantities of pyruvate for citrate synthesis. This leads to current debate of how cells can maintain the needed energy requirement for cellular growth and division while producing high-energy molecules such as ATP in a very inefficient manner in the presence of oxygen.



Cancer Research Reviews

Dang, C. V. (2010) Rethinking the Warburg Effect with Myc Micromanaging Glutamine Metabolism, *Cancer Research* 70, 859-862.

Figure 3. The Addition to the Warburg Effect

During a cellular proliferative state there needed to exist an alternative energy source to fill the energy void. As discussed previously proliferating cells in the presence of oxygen significantly increase their glucose consumption increasing the metabolic flux through the glycolytic pathway. The increased glycolytic flux predominantly leads to the formation of lactic acid generating small amounts of pyruvate. The generated pyruvate can then enter the TCA cycle forming citrate for fatty acid synthesis. The alternative energy source for proliferating cells is the catabolism of the amino acid glutamine. Glutamine consumption is increased during cellular proliferation. Glutamine is converted to glutamate in the glutaminase (GLS) reaction producing a free ammonium ion forming glutamate. Glutamate is subsequently reacted forming α -ketoglutarate. α -ketoglutarate is primary component for the TCA cycle which is able to produce the needed high-energy electron carriers for oxidative phosphorylation. It is important to note that this review studied cellular proliferation under *c-myc* induction and found that not only are glucose and glutamine's uptake increased, but the micro-RNA's miR23a and miR23b regulate glutaminase activity. Upon *c-myc* induction miR23a/b are repressed increasing the activity of the glutaminase enzyme.

GTPases sequestering them from the plasma membrane (20, 21). Dbl family proteins are oncogene products which share Dbl homology (DH) and pleckstrin homology (PH) domains and act as GEFs of the Ras and Rho family GTPases (22, 23). The increased activity of Dbl proteins enhances the activation of Rho-like small GTPases and influences cellular transformation (22). A recent publication by Erikson and Cerione linked GA to constitutively active Rho GTPases and oncogenic Dbl induced cellular transformation (8). They screened for potential drugs that attenuated the transformed phenotype produced by the over-expression of Dbl. The identified inhibitor of transformation (molecule 968) was shown to bind to and inhibit the glutaminase variant (GAC) isoform (8). Recent studies also suggest that over expression of the oncogene *myc* not only caused cellular transformation and increased anaerobic glycolysis, but also activated glutamine metabolism (10, 18). Upon *myc* induction, the micro-RNAs miR23a and miR23b are suppressed, resulting in increased GA expression and activity (24).

Previous studies have indicated that the N-terminal 72 amino acid sequence is removed following translocation of GA into the mitochondrion (2). hKGA₁₂₈₋₆₆₉, a construct that contains amino acids 128-669, was previously expressed to mimic the mature KGA isoform. A second construct, hKGA₁₂₄₋₅₅₁, that contains amino acids 124-551 was produced to delete the C-terminal sequences that are unique to the KGA and GAC isoforms. A third construct hKGA₂₂₁₋₅₃₂ was cloned to express an N-terminal and C-terminal truncation. hKGA₂₂₁₋₅₃₂ was recently crystallized in the presence of glutamate by the Structural Genomics Consortium (SGC)(PDB ID 3CZD). However, our construct differs from the SGC construct because it lacks a tobacco

etch virus (TEV) proteolytic cleavage tag which removes the N-terminal his₆-tag.

Figure 4 shows each of the constructs considered for kinetic study.

The hKGA truncated constructs were assayed in the presence of bis-2-(5-phenyllactamido-1,2,4-thiadiazol-2-yl)ethyl sulfide (BPTES). BPTES is a potent inhibitor of mammalian GA that inhibits rat KGA deletion constructs in μM concentrations (7). BPTES inhibits rKGA_{Δ1} as a mixed non-competitive inhibitor. Past inhibition studies have shown that BPTES does not bind to active site of mammalian KGA. Mammalian KGA exists as an inactive dimer in the absence of phosphate, but forms an active tetramer in the presence of phosphate(7, 25-27). Analytical ultra-centrifugation studies indicate that when BPTES binds, rat KGA_{Δ1} forms stable, but inactive tetramers (7). Inhibition studies suggest that BPTES binds allosterically to tetramers, thereby altering the conformation of the active complex. BPTES ability to inhibit KGA at low concentrations and with high specificity makes it a potential lead compound for drug studies. Other inhibitors such as 6-diazo-5-oxo-L-norleucine (DON), a glutamine analogue, inhibit mammalian GA in a competitive manner with less specificity. It has been suggested that DON preferentially interacts with active KGA; conversely, the inhibitor L-2-amino-4-oxo-5-chloropentanoic acid (CK) interacts with dimeric KGA. DON, but not CK, requires phosphate to inactivate mammalian GA. DON inhibition is enhanced in the presence of phosphate and inhibition by CK is decreased in the presence of phosphate (28, 29). Inhibitors like DON and CK require higher (mM) concentrations to inactivate mammalian KGA and

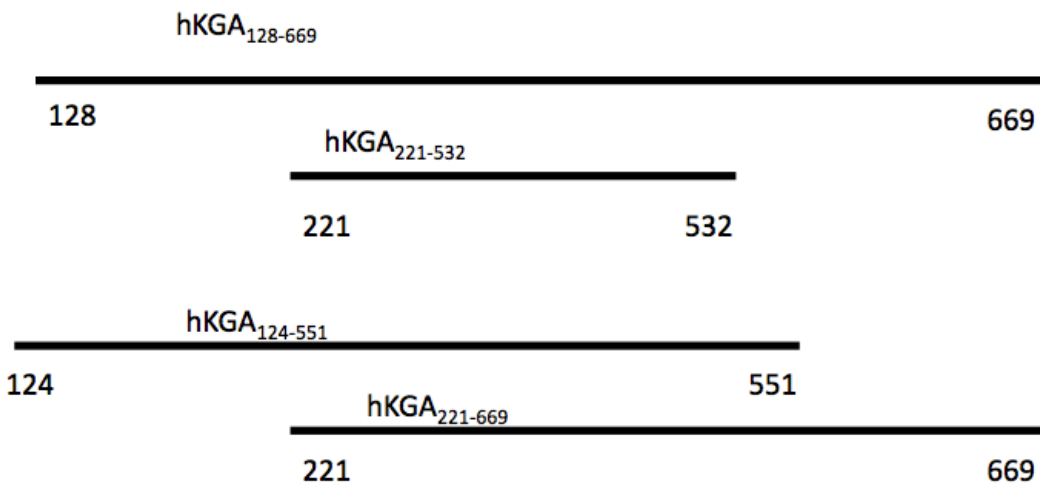


Figure 4. hKGA Constructs for Kinetic Analysis

The KGA constructs considered for kinetic study all include N-terminal His₆-tags. The hKGA₁₂₈₋₆₆₉ construct contains amino acids 128-669. This construct was produced to mimic a full length wild-type KGA because the first 100 amino acids are required to target KGA to the mitochondrion and is not retained in the mature protein. This construct contains the C-terminal sequence specific to the KGA isoform. The hKGA₂₂₁₋₅₃₂ is a N-terminal and C-terminal deletion construct, which was recently crystallized by the SGC. The hKGA₁₂₄₋₅₅₁ construct contains the N-terminal sequence of the mature KGA isoform but lacks the C-terminal sequence specific to the KGA enzyme. The last construct, hKGA₂₂₁₋₆₆₉, contains amino acids 221-669 and lacks the N-terminal sequence common the mature KGA isoform.

LGA activity and are not ideal lead compounds for drug targeting because they lack specificity and sufficient affinity for the mammalian KGA. Figure 5 contains the structures of the substrate and product of the glutaminase reaction along with the four inhibitors described above DON, CK, BPTES, and molecule 968.

Our approach is to study the hKGA₁₂₄₋₅₅₁ construct to determine if it retains properties characteristic of the mammalian GA. Basic activity will be established, as well as kinetic profiles for this construct, including the kinetic constants K_m , V_{max} , and K_i . Lastly, phosphate activation profiles will be compiled to determine if this deletion construct exhibits the phosphate-dependent activation and homodimerization that are unique characteristics of the mammalian KGA.

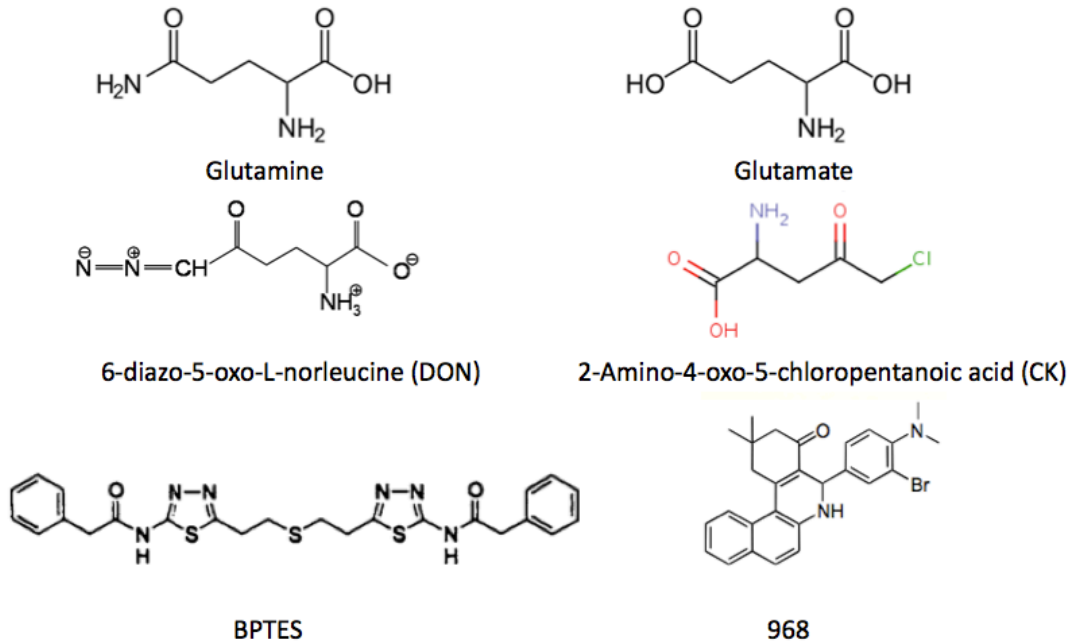


Figure 5. Structural Players

At the top are the structural representations of the substrate, glutamine, and the product, glutamate, of the glutaminase reaction. The inhibitors DON and CK are in the middle and share great structural homology to the glutaminase product and substrate. The last two inhibitors are BTPES and molecule 968 which are potent allosteric inhibitors of the glutaminase reaction.

Methods

Cloning of hKGA₁₂₄₋₅₅₁

hKGA₁₂₄₋₅₅₁ was cloned using hKGA 4 as the parent plasmid (30) which contains the complete hKGA coding region. Forward and reverse primers were used to amplify the desired segment. The sequence incorporated *NdeI* and *BamHI* restriction sites at the 5' and 3' ends, respectively. The insert was shuttled through the pGEM-T easy vector and then ligated into the pET-15b expression vector. The plasmid, pET-15b rKGA₁, was cut with *NdeI* and *BamHI* restriction enzymes to remove the rKGA₁ insert. pET-15b rKGA₁ is an expression plasmid containing the rat isoform of KGA lacking the sequence encoded by exon 1. The insert (1295 bp) containing hKGA₁₂₄₋₅₅₁ sequence was cut out of the pGEM-T easy plasmid and ligated into the pET-15b vector fragment (5700 bp) using Quick Stick Ligation kit resulting in a pET-15b hKGA₁₂₄₋₅₅₁ plasmid. DNA sequencing across the entire insert confirmed the plasmid identity.

Protein expression and purification

Recombinant protein expression of pET-15b hKGA₁₂₄₋₅₅₁, an N- and C-terminal truncation of human glutaminase, was performed using *Escherichia coli* strain BL-21 (DE3) that contained the Rosetta pRARE plasmid. The *E. coli* strain was obtained from the Structural Genomics Consortium (SGC) at the Karolinska Institutet. Cell cultures were grown in 6 L of medium at 37°C to an O.D.₆₀₀ of 1.0-1.5 and then cooled to 18°C before being induced with 0.5 mM IPTG. Cultures were harvested the

following morning by centrifugation at 4000 rpm at 4°C for 30 minutes. Harvested cell pellets were resuspended in 50 mL of lysis buffer containing 300 mM KCl, 10% glycerol (v/v), 10 mM Tris-Cl, pH 8.0, 10 mM potassium phosphate, 10 mM imidazole, 0.5 mM Tris(2-carboxyethyl)phosphine hydrochloride (TCEP), a potent and stable reducing agent, and one tablet of Complete Protease Inhibitor Cocktail (Roche). Resuspended cell pellets were then stored in a -80°C freezer. Cell pellets were thawed in an ice water bath and disrupted by sonication in the presence of 2000-4000 units of Benzonase. The lysate was centrifuged at 35,000 rpm at 4°C for 25 minutes. The supernatant was pooled and filtered through a 0.22-micron syringe filter. The filtered supernatant was then manually loaded onto a 5 mL HiTrap nickel-chelating column (Amersham Biosciences) using a peristaltic pump with a flow rate of approximately 1.0 mL/minute. Immobilized metal affinity chromatography (IMAC) and size exclusion chromatography (SEC) were accomplished using an AKTA FPLC apparatus. Elution of the N-terminal His₆-tagged hKGA₁₂₄₋₅₅₁ was accomplished by using an increasing gradient of 75 mM to 400 mM imidazole in 300 mM KCl, 10 mM Tris-Cl, pH 8.0, 10 mM potassium phosphate, 10% glycerol (v/v), and 0.5 mM TCEP. Fractions were collected in 3.0 mL volumes and assayed using 10% SDS-PAGE. The fraction containing the hKGA₁₂₄₋₅₅₁ was loaded manually onto a S200 Superdex™ 16/60 gel filtration column and eluted using 300 mM KCl, 10 mM Tris pH 8.0, 100 mM potassium phosphate, 10% glycerol (v/v), and 0.5 mM TCEP at a flow rate of 1.0 mL/min. Fractions were collected in 3.0 mL volumes and assayed by 10% SDS-PAGE. Purified recombinant protein was stored in 15 mL falcon tubes at 4°C. Fractions were collected throughout the expression

and purification to assess the enrichment and recovery of the hKGA₁₂₄₋₅₅₁. The activity and specific activity of the lysate, supernatant, and purified fraction was measured using a modified version of the two-step kinetic assay describe previously (13).

Kinetic Assays

hKGA₁₂₄₋₅₅₁ activity was determined using a two-step assay that was performed using 96-well plates in a final volume of 227 µL per well (7). Each well contained 10 µL of 2X stock assay mix #1 containing 300 mM potassium phosphate, 0.4 mM EDTA, 100 mM tris acetate, pH 8.6, and 10 µL of 40 mM glutamine. The assay was started by adding 5 µL of an appropriate dilution of the recombinant hKGA₁₂₄₋₅₅₁ to 20 µL of the complete assay mix. The reaction was incubated for 10 minutes in a 37°C incubator and stopped by the addition of 2 µL of 3N HCl. Next, 200 µL of assay mix #2 containing 0.4 mg/mL bovine liver glutamate dehydrogenase (Sigma), 80 mM tris acetate, pH 9.4, 200 mM hydrazine, 2.5 mM ADP, and 0.2 mM NAD⁺ was added. Reaction samples were incubated for 35 minutes at room temperature. Absorbance at 340 nm was read using a Wallac Victor^{3V} plate reader (PerkinElmer). Each sample absorbance was measured against a blank in which the 3N HCl was added immediately before the addition of hKGA₁₂₄₋₅₅₁. In the first reaction glutamine is converted into glutamate and an ammonium ion. The addition of 3 N HCl denatures the glutaminase before the secondary reaction mixture is added. In the second reaction, bovine liver glutamate dehydrogenase catalytically converts glutamate, from the first reaction, into α-ketoglutarate producing an equivalent amount of

NADH per molecule of glutamate. Hydrazine reacts with α -ketoglutarate, forming a hydrazide to ensure that the reaction proceeds to completion. To study the inhibition of hKGA₁₂₄₋₅₅₁, a GA inhibitor (Gilford Pharmaceuticals), bis-2- (5-phenyllactamido-1, 2,4-thiadiazol-2-yl) ethyl sulfide (BPTES), is added to the primary reaction in a 1 μ L volume to yield a final concentration of 0.1 μ M, 0.3 μ M, 0.6 μ M, 1.0 μ M, and 2.0 μ M. Since BPTES is dissolved in DMSO, a DMSO control was performed by adding 1 μ L of DMSO to reaction mixture before the addition of hKGA₁₂₄₋₅₅₁. Activity (units/mL) and specific activity (units/mg) were calculated using Excel software (Microsoft). Data analysis to determine the kinetic constants, K_m and V_{max} , were performed using KaleidaGraph software (Synergy Software) to fit the Michaelis-Menten equation:

$$v = \frac{V_{max} \cdot [Gln]}{[Gln] + K_m}$$

where the [Gln] is the substrate concentration in mM. Glutamine saturation profiles were conducted with five replicates of each concentration between 0.5 mM to 80 mM glutamine. To study the inhibition of hKGA₁₂₄₋₅₅₁ by BPTES, glutamine saturation profiles were performed in the presence of DMSO, 0.1 μ M, 0.3 μ M, 0.6 μ M, and 1.0 μ M BPTES. To determine the K_i for BPTES, the apparent V_{max} and apparent K_m were plotted against the concentration of BPTES using KaleidaGraph software to fit the equations:

$$\text{Apparent } V_{max} = \frac{V_{max}}{(1 + [I]/K_i)}$$

$$\text{Apparent } K_m = \frac{K_m}{(1 + [I]/K_i)}$$

where the $[I]$ is equal to the concentration of BPTES.

Phosphate activation profiles were completed in replicates of five using a range of phosphate concentrations (0.5 mM to 150 mM) in the presence of 1 μ L DMSO, 0.5 μ M, 1.0 μ M, 3.0 μ M, and 10 μ M BPTES. The Hill coefficient and $K_{0.5}$ were determined using KalidaGraph software to perform a non-linear least squares fit to the Hill equation

$$v_o/V_{max} = [P]^h/(K_{0.5} + [P]^h)$$

where v_o/V_{max} is the fractional saturation of hKGA₁₂₄₋₅₅₁ with phosphate, h is the Hill coefficient, $K_{0.5}$ is the dissociation constant, and $[P]$ is the concentration of phosphate.

Size Exclusion Gel Filtration Chromatography

Gel filtration chromatography was performed using a 15-mL Bio-Slect SEC 250 column with an AKTA FPLC system at 4°C (7). A 80- μ L sample containing 1.0 mg/mL, roughly 20 μ M, of recombinant hKGA₁₂₄₋₅₅₁ was applied to the SEC column

that was pre-equilibrated in 300 mM KCl, 10 mM tris-Cl, pH 8.0, 10% glycerol (v/v), and 0.5 mM TCEP with varying concentrations of potassium phosphate. hKGA₁₂₄₋₅₅₁ was concentrated in a 20 mL Viaspin 3.0 kDa MW cut-off concentrator by centrifuging in a swinging bucket rotor (Beckman) at 1207 x g at 4°C. Concentrated samples were dialyzed against SEC buffer containing 0 mM potassium and 100 mM potassium phosphate (Sigma) for 3 to 5 hours at 4°C. Dialyzed samples were loaded onto the Bio-Slect 250 column in 80 uL volumes and the elution profile was determined by measuring the absorbance at 230 nm.

Bio-Rad gel filtration standards were used to calibrate the gel filtration column to assess apparent molecular weights. The standard contains bovine thyroglobulin (670,000 Da), bovine γ -globulin (158,000 Da), chicken ovalbumin (44,000 Da), horse myoglobin (17,000 Da), and vitamin B₁₂ (1,350 Da). The mixture was rehydrated using water and loaded onto the column using a volume of \leq 1% of the total column volume. The elution of the standards was tracked using absorbance at 230 nm and 280 nm.

Size Exclusion Chromatography-Multi Angle Light Scattering (SEC-MALS)

Light scattering experiments were performed using Wyatt Technologies DAWN® HELEOS™ II in tandem with Optilab® T-rEX detectors coupled to an AKTA FPLC system connected to S200 Superdex™ 10/30 gel filtration column. The SEC column was equilibrated in SEC-MALS buffer containing 5 mM L-arginine, 300 mM KCl, 10 mM Tris pH 8.0, 2% glycerol (v/v), and 0.5 mM TCEP with either 0 mM or 150 mM phosphate. Each SEC-MALS buffer was filtered sequentially using a 0.22-

micron filter and 0.10-micron filter. Recombinant hKGA₁₂₄₋₅₅₁ was purified as discussed above with the addition of a third chromatography step. Ion exchange chromatography was performed after the nickel IMAC purification step. Fractions containing sample were pooled from the nickel purification and diluted 10-fold in Q-column buffer A containing 10 mM Tris pH 8.0, 10% glycerol (v/v), 0.25 mM TCEP, and 10 mM potassium phosphate. The sample was loaded manually, using a peristaltic pump at a flow rate of 2.0 mL/min, onto a Hi-Trap Q (GE Healthcare) ion exchange column equilibrated in Q-column buffer A. The column was then connected to an AKTA FPLC and the target protein was eluted off the column using an increasing KCl gradient. Fractions were collected in 5 mL while a chromatogram tracked absorbance of the eluant at 280 nm. Samples containing hKGA₁₂₄₋₅₅₁ were assayed using 10% SDS-PAGE and then concentrated into two separate fractions of less than 3.0 mL and loaded onto S200 16/60 gel filtration column as described above. Due to the instability of hKGA₁₂₄₋₅₅₁ at high concentrations, the S200 16/60 gel filtration was performed twice to ensure greater stability and lower concentrations of hKGA₁₂₄₋₅₅₁ per fraction. Fractions were assayed by 10% SDS-PAGE and then pooled for concentration. Purified hKGA₁₂₄₋₅₅₁ was concentrated as described above to roughly 1.0 mg/mL. The concentrated samples were loaded onto the SEC-MALS AKTA FPLC system with and without 2.0 μM BPTES in 0 mM phosphate and 150 mM phosphate at a flow rate of 0.3 mL/min. A chromatogram tracked the absorbance of each sample at 280 nm or 230 nm. Analysis of SEC-MALS data was performed using ASTRA® software.

Results

I initially planned to characterize the hKGA₂₂₁₋₅₃₂ form of glutaminase. However, expression and purification of recombinant hKGA₂₂₁₋₅₃₂ was problematic. Analysis of the expression by SDS-PAGE indicates that most of the enzyme remains insoluble due to the presence of a very intense band in the pellet fraction (data not shown). The small yield that is produced from purification does not appear to be stable in solution. It rapidly lost activity and precipitated out of solution. Buffer changes and pH changes have not produced soluble enzyme long enough to study its kinetic behavior. Further study found that there was a C-terminal degradation of hKGA₂₂₁₋₅₃₂ during expression and purification. This was confirmed by western blot (data not shown) as two bands reacted with the GA antibody just below the 50-kDa marker. In attempt to alleviate these problems, the plasmid used by the SGC to determine the crystal structure was obtained. This hKGA construct also contained amino acids 221-532 but contains an N-terminal proteolytic cleavage sequence that can be used to remove the His₆-tag from the construct. Expression and purification of this newly obtained construct was also problematic. The hKGA₂₂₁₋₅₃₂ construct was soluble in very small amounts and precipitated from solution prior to purification attempts. As seen with the previous construct, it was difficult to determine enzymatic activity as the sample precipitated out of solution. Due to these problems, I used the hKGA₁₂₄₋₅₅₁ construct and had improved data collection.

Recombinant protein expression and purification

The hKGA₁₂₄₋₅₅₁ pET-15b plasmid was transformed into the BL-21 (DE3) strain of *E. coli* and plated on LB media containing 100 µg/mL ampicillin and 34 µg/mL chloramphenicol. A 1-mL aliquot of a 5-mL overnight culture was added to each of the two 1-L flasks of 2xYT growth media. The uninduced culture was grown at 37°C until the O.D.₆₀₀ reached 1.0 to 1.5. The culture was then cooled to 18°C before being induced with 0.5 mM IPTG. The quality of induction can be seen in Figure 6. The first lane shows the uninduced sample where there is minimal band intensity near the 50-kDa marker. In the induced sample (lane two), there is a very intense band just below the 50-kDa marker. This shows that there is very little leaky transcription of the transformed plasmid and that the target protein is effectively induced. Comparison of the pellet fraction and supernatant fractions indicate that more than half of the protein remains soluble and that sonication is an adequate cell disruption method. The supernatant was subsequently filtered and manually loaded onto a 5-mL nickel column equilibrated in buffer A (300 mM KCl, 10 mM tris-Cl, pH 8.0, 10 mM potassium phosphate, 10% glycerol (v/v), and 0.5 mM TCEP). The His₆-tagged hKGA₁₂₄₋₅₅₁ was eluted from the column using an increasing imidazole gradient. Column fractions 24-26 (Figures 7, 8) contain an intense band near the 50-kDa marker that correlates with the elution profile of the nickel column (Figure 7). The column eluant was collected in 3-mL fractions and no further concentration was required. Column fraction 25 was then manually loaded onto a Superdex S200 16/60 column equilibrated in gel filtration buffer (300 mM KCl, 10 mM Tris pH 8.0,

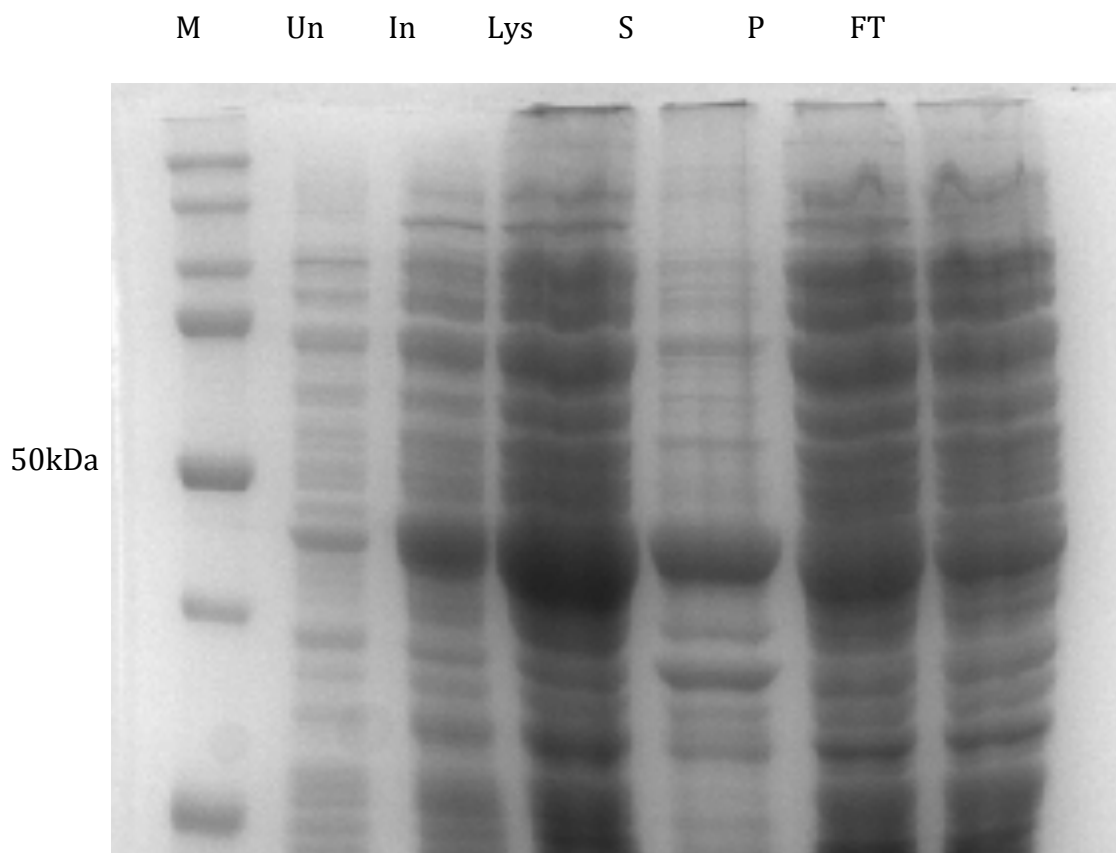


Figure 6 Expression analysis of hKGA₁₂₄₋₅₅₁ construct

10% SDS-PAGE was performed to track the expression and purification of hKGA₁₂₄₋₅₅₁. The un-induced cell culture (Un) was induced using 0.5 mM IPTG (In) as shown in lanes 2 and 3 respectively. The solubility of hKGA₁₂₈₋₅₃₂ in lysis buffer is represented by the lysate (Lys) (lane 4), pellet (P) (lane 5), and supernatant (S) (lane 6) fractions. The supernatant was then manually loaded onto 5-mL nickel column and the flow through (FT) was collected (lane 7).

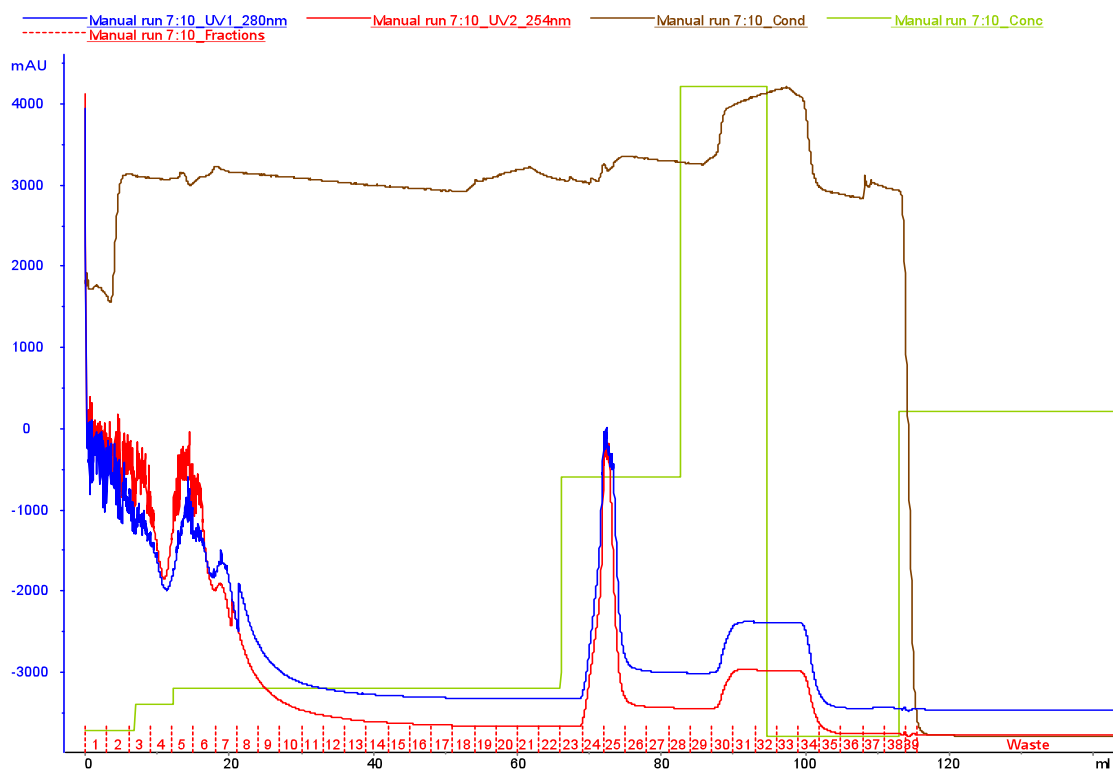


Figure 7. Elution Profile of hKGA 124-551 from a 5-mL nickel column

The nickel column was equilibrated in buffer A and the cell supernatant was manually loaded on the column. The column was then placed onto the AKTA FPLC system where an increasing imidazole gradient (green line) was used to elute off the his₆-tagged glutaminase in 3-mL fractions. 1% to 7.5 % buffer B (75 mM imidazole) was run for 20 column volumes until the A_{280} leveled off near zero. The concentration of imidazole was then increased to 400 mM (40% buffer B) to elute the target protein in one step. Once the A_{280} (blue line) leveled off 100% buffer B (1M imidazole) was run for 5 column volumes to remove any proteins still bound to the nickel resin. From this chromatogram samples were collected from column volumes 24-26 and assayed by 10% SDS-PAGE.

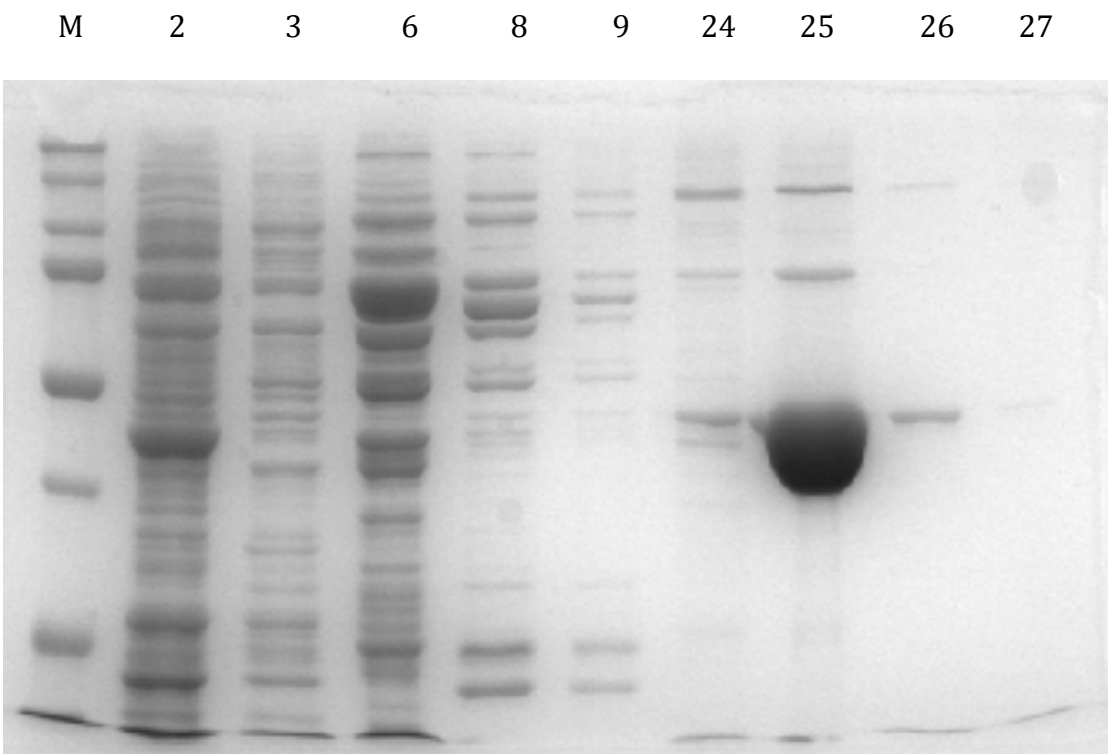


Figure 8 IMAC purification by nickel affinity chromatography

Analysis of IMAC purification by 10% SDS-PAGE shows that His₆-tagged hKGA₁₂₄₋₅₅₁ binds with high affinity to the nickel column. Fraction numbers 2, 3, 6, 8, and 9 show column fractions containing protein contaminants eluted by 10 mM to 75 mM imidazole. Column fraction 24-26 (lanes 7-9) show how effective the elution of the target protein was completed in one step at 400 mM imidazole. Column fraction 25 was manually loaded onto a pre-equilibrated S200 16/60 size exclusion column for further purification.

100 mM potassium phosphate, 10% glycerol (v/v), and 0.5 mM TCEP). The fractions were collected in 3-mL volumes at a flow rate of 1.0 mL/minute. The gel filtration purification was successful as seen in column fractions 20-24 (Figures 9, 10) where there is an intense band just below the 50-kDa marker. Furthermore, when comparing Figure 8 to Figure 10 there is an apparent removal of contaminating bands indicating that gel filtration is an effective chromatography step for the further purification of hKGA₁₂₄₋₅₅₁. SDS-PAGE analysis correlates well with the gel filtration chromatogram as seen in both the nickel IMAC and SEC purification steps (Figures 7 and 9, respectively). Lastly, there is a broad peak and significant tail in the gel filtration profile (Figure 9 and 10) indicating that the hKGA₁₂₄₋₅₅₁ may undergo association and dissociation during the gel filtration chromatography.

hKGA₁₂₄₋₅₅₁ Activity

The activity of hKGA₁₂₄₋₅₅₁ was tracked throughout the purification. As seen in Table 1, the specific activities between the lysate and supernatant fractions, 8.4 U/mg and 10 U/mg respectively, were similar. The specific activity of the hKGA₁₂₄₋₅₅₁ recovered from the nickel column was increased 60-fold (590 U/mg). The purification was accomplished with a recovery of approximately 20% of the total activity expressed in the initial lysate. The specific activity of the purified hKGA₁₂₄₋₅₅₁ is similar to the specific activity of full-length rKGA and a truncated version of the rat KGA (7).

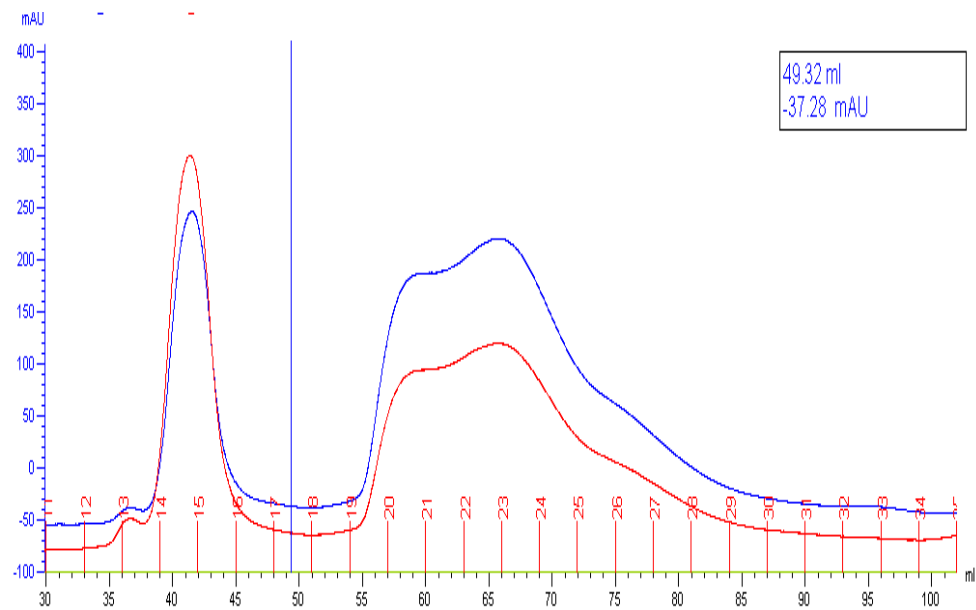


Figure 9 Gel filtration chromatogram of hKGA₁₂₄₋₅₅₁ purification

hKGA₁₂₈₋₅₃₂ was eluted at a flow rate of 1.0 mL/min and monitored by A₂₈₀ (blue line) and A₂₅₄ (red line). The chromatogram shows a very sharp peak corresponding to column fractions 14 and 15. Protein samples were collected from column fractions 13-16, 19-28, and analyzed by 10% SDS-PAGE.

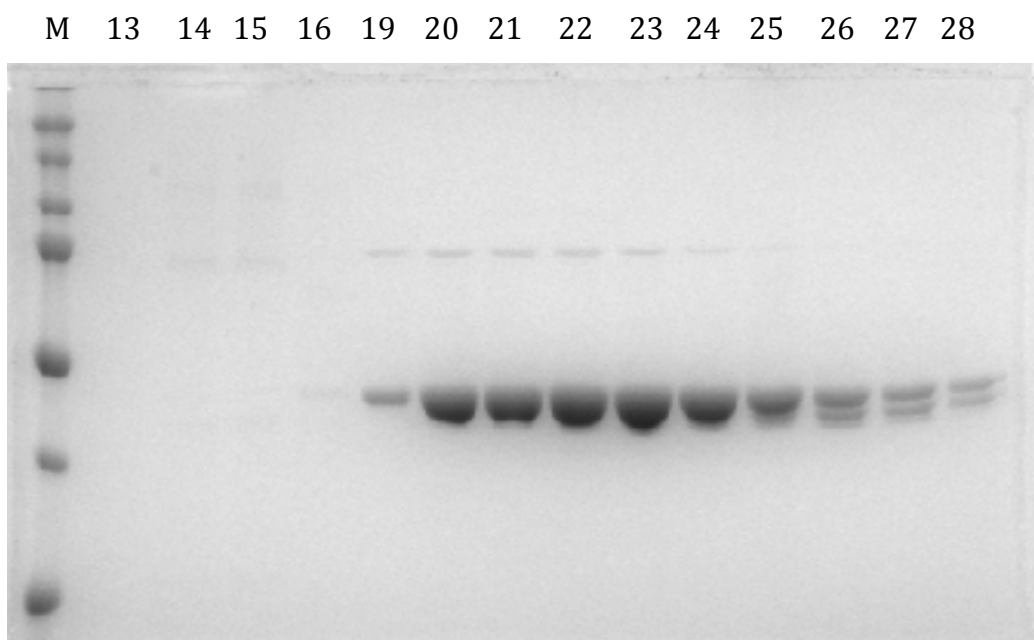


Figure 10 Purification analysis of hKGA₁₂₄₋₅₅₁ using gel filtration chromatography

Column fraction 25 from the nickel affinity chromatography was manually loaded onto S200 16/60 Superdex column equilibrated in 300 mM KCl, 10 mM Tris pH 8.0, 100 mM potassium phosphate, 10% glycerol (v/v), and 0.5 mM TCEP at a flow rate of 1.0 mL/min. Fractions were collected in 3.0-mL volumes and assayed by 10% SDS-PAGE. Column fractions 19 through 28 contain the target protein indicated by the band intensity just below the 50-kDa marker. Column fractions 20-24, which have the most intense bands, were used for the kinetic analysis.

Table 1 Purification of recombinant hKGA₁₂₈₋₅₃₂

Sample	Total volume (mL)	U/mL	Total Activity Units	Protein mg/mL	Total mg	U/mg
Lysate	31.6	263	8311	31.2	985	8.4
Supernatant	26.8	261	6995	22.9	614	10
hKGA ₁₂₈₋₅₃₂ nickel affinity chromatography fraction 25	3.0	539	1617	0.9	2.7	591

The activity of hKGA₁₂₄₋₅₅₁ was monitored throughout the purification. The activity (units/mL) and specific activity (units/mg) increase throughout the purification as seen in columns 2 and 6. The protein concentration was assayed by the Bradford method (column 4). The total protein (column 5) was calculated by multiplying the concentration by the total volume of the sample (column 1). The total activity (column 3) was calculated by multiplying the activity (column 2) by the total volume of sample (column 1). The activity assay was performed using the method of Kenny, J. *et al.* 2003 where the total volumes of the assay are larger and not run in a 96-well micro plate.

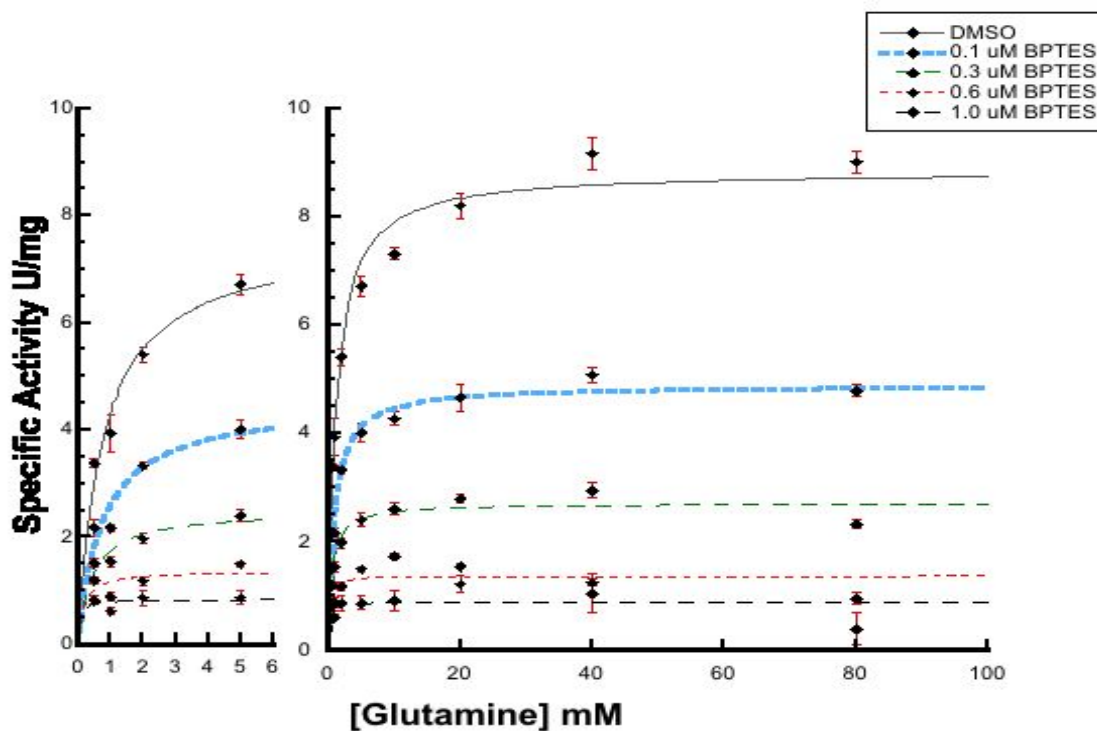
Kinetics

To determine the kinetic properties and type of inhibition by BPTES, glutamine saturation profiles were performed using DMSO or 0.1, 0.3, 0.6, and 1.0 μM BPTES in DMSO. Figure 11 shows the increase in hKGA₁₂₄₋₅₅₁ specific activity with increasing concentrations of glutamine at 10 mM or 30 mM phosphate. The data fit to a hyperbolic saturation profile, and at each increasing concentration of BPTES the specific activity was reduced. Figure 11a shows glutamine saturation data in the presence of BPTES at 10 mM phosphate, whereas Figure 11b shows the glutamine saturation data at 30 mM phosphate. The observed K_m for hKGA₁₂₄₋₅₅₁ in the presence of DMSO at 10 mM phosphate was $1.2 \text{ mM} \pm 0.2$ which was similar to the K_m of $1.5 \text{ mM} \pm 0.13$ at 30 mM phosphate. In both phosphate concentrations the observed K_m and the observed V_{max} decreased as the concentration of BPTES increased. The data shows that there is a significant decrease in V_{max} and a slight decrease in K_m indicative of uncompetitive inhibition or a mixed inhibition model. A detailed determination of K_m and V_{max} values can be seen in Supplemental Table 1 in Appendix 1. This conclusion is better illustrated in the double reciprocal plots (Figure 12a and 12b). When comparing the DMSO control to 0.1 μM BPTES at 10 mM phosphate, the inhibition appears to be mixed non-competitive inhibition (Figure 12a). However, at 30 mM phosphate and 0.1 μM BPTES the model of inhibition appears to be uncompetitive (Figure 12b). At higher concentrations of BPTES, the inhibition profiles fit best to an uncompetitive model at both 10 and 30 mM phosphate. Strict non-competitive inhibition occurs when the inhibitor binds to a site separate from the substrate binding site, resulting in a decrease of enzymatic

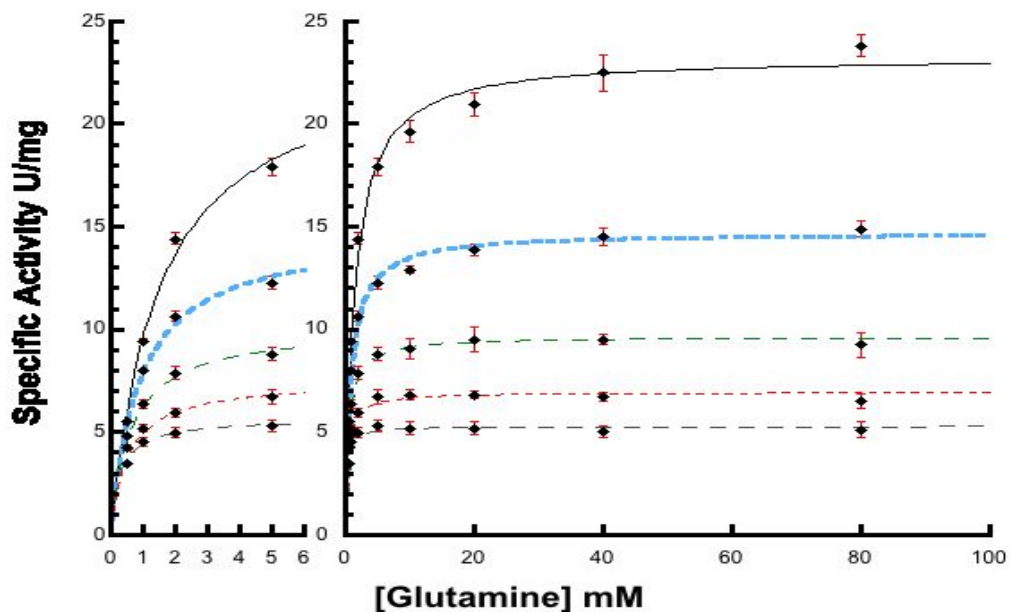
turnover, while the K_m remains unchanged. Uncompetitive inhibition occurs when the inhibitor binds to the enzyme-substrate complex and alters the K_m and catalytic activity to a similar extent. A mixed inhibition model occurs when the inhibitor can bind free enzyme and enzyme-substrate complex and produces differential effects on the catalytic activity and the K_m for substrate. For a strict non-competitive inhibition, all the lines of the double reciprocal plots should intercept on the x-axis indicating the K_m remains unchanged, and each line should intercept the y-axis at higher values for higher inhibitor concentrations indicating the V_{max} decreases. On the other hand, typical uncompetitive inhibition should yield parallel lines on the double reciprocal plot that intersect the x-axis and y-axis at different positions indicating similar changes in both V_{max} and K_m . Double reciprocal plots of mixed inhibition result in the lines intersecting before the y-axis indicating differential changes in both V_{max} and K_m .

The K_i for BPTES was determined at both 10 mM and 30 mM phosphate by plotting the apparent V_{max} and the apparent K_m against the concentration of BPTES (Figures 13a and 13b, respectively). At 10 mM phosphate the K_i determined by plotting the apparent V_{max} was $0.14 \pm 0.01 \mu\text{M}$, and by plotting the apparent K_m the K_i was $0.21 \pm 0.06 \mu\text{M}$. At 30 mM phosphate the K_i determined by plotting the apparent V_{max} was $0.24 \pm 0.03 \mu\text{M}$, and plotting the apparent K_m the K_i was $0.16 \pm 0.02 \mu\text{M}$. Large changes in K_i at either phosphate concentration would support a mixed inhibition and non-competitive inhibition model; however, the data indicate that the calculated K_i values do not change significantly between phosphate conditions.

11a

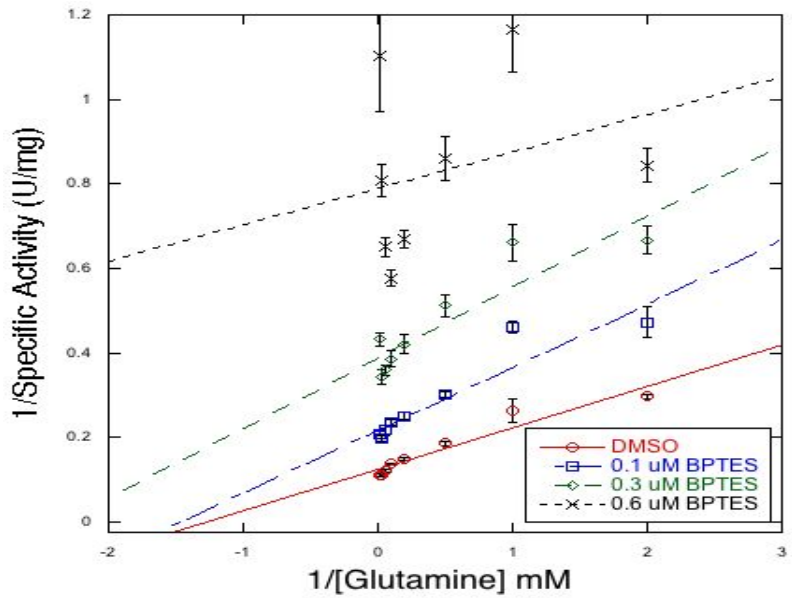


11b

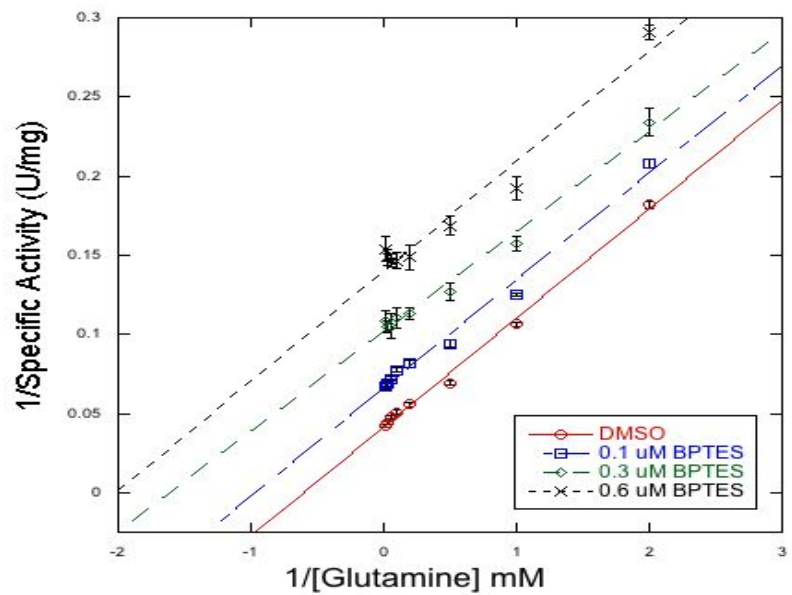
**Figure 11 Glutamine saturation profiles in the presence of BPTES**

Glutamine saturation profiles were performed in 10 mM (panel A) and 30 mM (panel B) phosphate with increasing concentrations of BPTES. The data are plotted using KalidaGraph software and fit to the Michaelis-Menten equation using a non-linear regression. The specific activity in units/mg was plotted against the concentration of glutamine. Data are the mean \pm standard error of five replicates.

12a

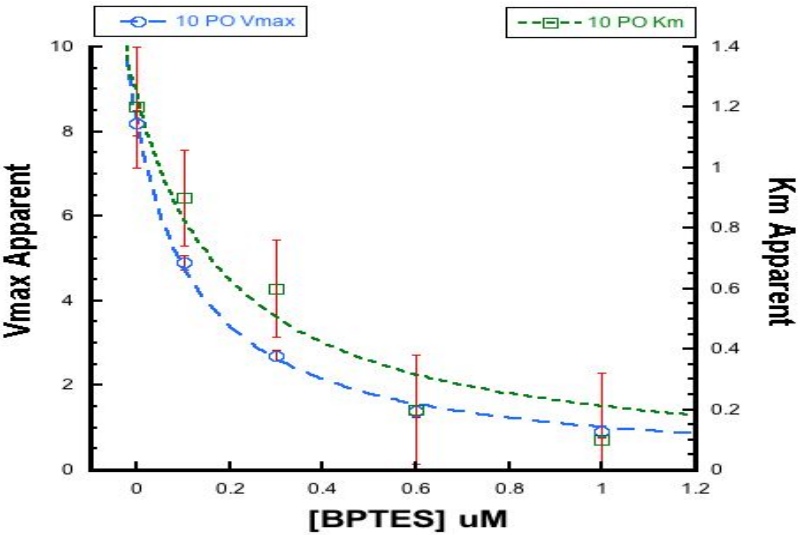


12b

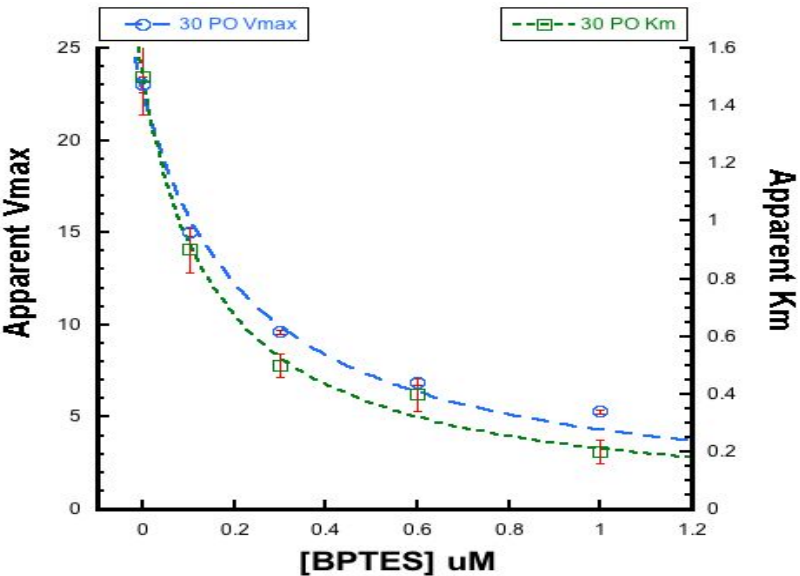
**Figure 12 Double-reciprocal plots of hKGA₁₂₄₋₅₅₁ activity**

Lineweaver-Burke double-reciprocal plot transformations of the glutamine saturation data were plotted for hKGA₁₂₄₋₅₅₁ in the presence of 10 mM phosphate (panel A) or in the presence of 30 mM phosphate (panel B). Increasing concentrations of BPTES was added from 0.1 μM to 1.0 μM. The lines represent a linear curve fit of the reciprocal mean specific activity versus the reciprocal concentration of glutamine.

13a



13b

**Figure 13 Determination of K_i**

The K_i for hKGA₁₂₄₋₅₅₁ was determined by plotting both the apparent V_{max} (panel A) and apparent K_m (panel B) versus the concentration of BPTES using KalidaGraph software. In panel A the dashed blue line represents the apparent V_{max} used to calculate the K_i for BPTES at 10 mM phosphate ($0.14 \mu\text{M} \pm 0.01$) and the dashed green represents the apparent K_m used to calculate the K_i for BPTES at 10 mM phosphate ($0.21 \mu\text{M} \pm 0.06$). In panel B the dashed blue line represents the K_i for 30 mM phosphate ($0.24 \mu\text{M} \pm 0.03$) calculated using the apparent V_{max} and the dashed green line represents the K_i for 30 mM phosphate ($0.16 \mu\text{M} \pm 0.02$) calculated using the apparent K_m . The left y-axis is the apparent V_{max} and the right y-axis is the apparent K_m .

In the presence of 10 mM and 30 mM phosphate, the K_i remains nearly unchanged and within their respective statistical standard error measurements. This observation supports an uncompetitive model of inhibition over a mixed inhibition model or non-competitive inhibition model, because changes in BPTES produce equivalent effects on the apparent K_m and the apparent V_{max} . The data clearly exclude competitive and strict non-competitive models of inhibition. However, the data is not sufficient to clearly discriminate between an uncompetitive and mixed inhibition model at low concentrations of phosphate, and it appears that the mechanism of inhibition may be dependent upon the phosphate concentration. It is clearly evident that in the 30 mM phosphate double-reciprocal plot, the mechanism of inhibition is strictly uncompetitive.

Phosphate activation profiles were performed in the presence of 20 mM glutamine in the absence or presence of BPTES (Figure 14). The specific activity of hKGA₁₂₄₋₅₅₁ increased as the concentration of phosphate increased. As the concentration of BPTES increased the overall specific activity of hKGA₁₂₄₋₅₅₁ decreased. However, when the data were fit to the Hill equation using KalidaGraph software, the overall profiles appear to be hyperbolic and the saturation profiles exhibit a slight cooperativity (Table 2) as previously observed with other mammalian constructs (7). The $K_{0.5}$ values for phosphate increased significantly in the presence of BPTES suggesting that phosphate and BPTES compete for binding to hKGA₁₂₄₋₅₅₁. The Hill coefficient also increased as the concentration of BPTES increased. This is evident in the activation profile (Figure 14) where the 10 μ M BPTES plot is sigmoidal.

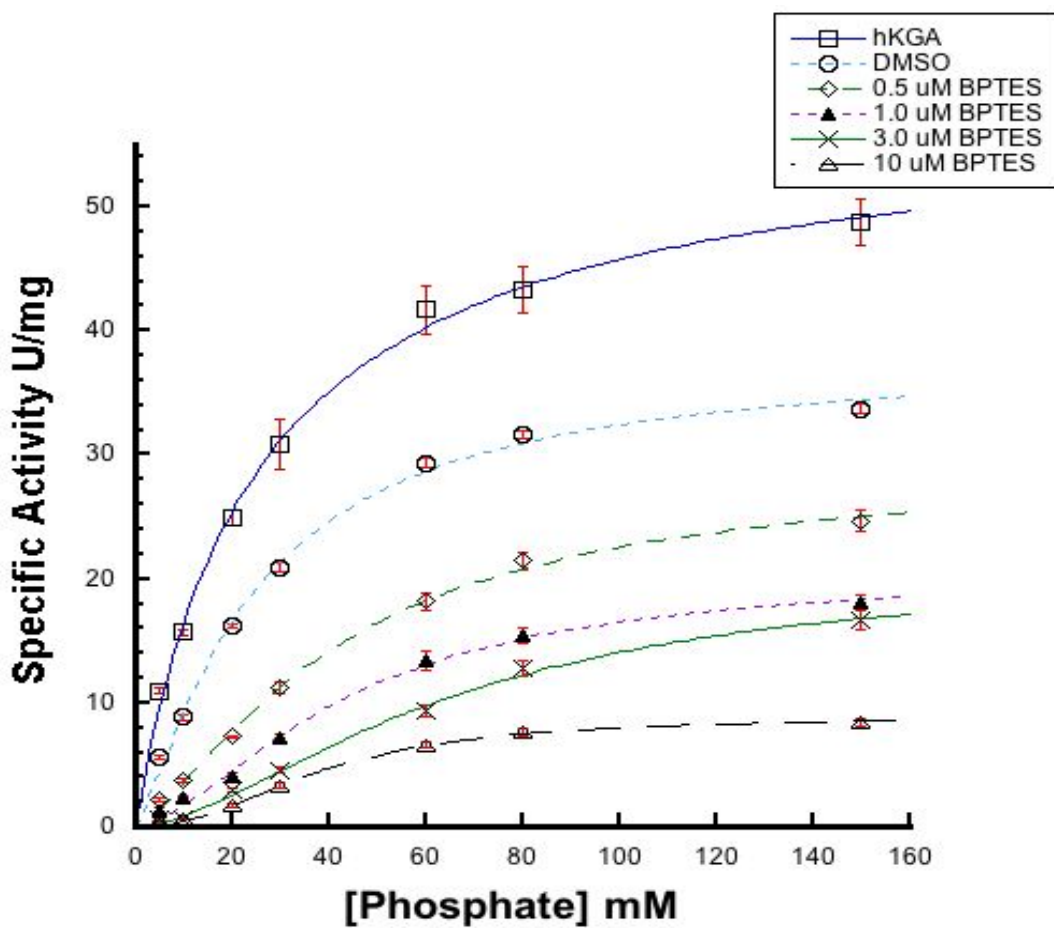


Figure 14 Phosphate activation profile of hKGA₁₂₄₋₅₅₁

Phosphate activation profiles were produced in the absence and presence of BPTES over a range of phosphate concentrations (x-axis). The y-axis is the specific activity of hKGA₁₂₄₋₅₅₁ in the presence of the DMSO control at increasing concentrations of BPTES. The data are the \pm standard error of five measurements at each phosphate concentration. The derived kinetic constants are summarized in Table 2.

Table 2 Calculated kinetic constants from the phosphate activation profile

Sample	$K_{0.5}$ (mM)	$Vmax$	Hill Coefficient
DMSO	56 ± 16	38.0 ± 1.8	1.3 ± 0.1
0.5 μ M BPTES	180 ± 60	29.0 ± 1.7	1.4 ± 0.1
1.0 μ M BPTES	500 ± 300	21.0 ± 1.5	1.6 ± 0.2
3.0 μ M BPTES	1000 ± 500	21.0 ± 1.7	1.6 ± 0.2
10 μ M BPTES	3000 ± 2000	9.0 ± 0.3	2.2 ± 0.2

The overall activity for each concentration of BPTES increased as the concentration of phosphate increased indicating increasing amounts of phosphate increase the V_{max} . Figure 14 clearly depicts the decrease in V_{max} . As the inhibitor concentration is increased, the hyperbolic curves plateau at lower specific activities.

Gel Filtration Chromatography

Gel filtration chromatography was performed using concentrated hKGA₁₂₄₋₅₅₁ in the absence and presence of BPTES at 0 mM and 100 mM phosphate (Figure 15a and 15b). At 0 mM phosphate, in the absence of BPTES, the sample has a longer retention volume. The hKGA₁₂₄₋₅₅₁ elutes from the column with a shorter retention time in the presence of 2 μ M and 10 μ M BPTES (Figure 15a). Comparing Figure 15a to 15b shows that 100 mM phosphate does not shift the elution profile in the absence of BPTES to the left decreasing the retention volume. In the presence of 100 mM phosphate, the addition of 2 μ M or 10 μ M BPTES produced a shift in the elution profiles, similar to the elution profiles in the absence of phosphate.

The apparent molecular weight of the hKGA₁₂₄₋₅₅₁ was determined by calibrating the Bio Silect 250 column with Bio Rad gel filtration standards. Plotting the elution volume on the y-axis and the log molecular weight on the x-axis, as seen in Figure 16, generated a linear standard curve fit. From the standard curve the molecular weights of hKGA₁₂₄₋₅₅₁ were calculated. In the absence of phosphate and BPTES the apparent molecular weight was 103-kDa and in the presence of 100 mM phosphate the apparent molecular weight was 124-kDa. As the concentration of BPTES increased so did the molecular weights in both the absence and presence of

phosphate. The apparent molecular weight at 2 μ M and 10 μ M BPTES in the absence of phosphate was 226-kDa and 241-kDa, respectively. In the presence of 100 mM phosphate the apparent molecular weight at 2 μ M and 10 μ M BPTES was 245-kDa and 284-kDa. The calculated molecular weight of the hGKA₁₂₄₋₅₅₁ monomer is 46-kDa. These data suggest that in the absence or presence of phosphate, hGKA₁₂₄₋₅₅₁ exists in a dimer. However, when BPTES is added, the molecular weight shifts to a tetramer and or higher oligomeric forms.

Size Exclusion Chromatography-Multi Angle Light Scattering

Multi-angle light scattering experiments of hGKA₁₂₄₋₅₅₁ did not produce quality results. Light scattering at 280 nm in the absence of BPTES and in 0 mM phosphate generated preliminary data of a 100-kDa species. The addition of the 2 μ M BPTES, at 0 mM phosphate, shifted the molecular weight to about a 200-kDa form; however, both of these experiments had large errors, in their measurements (data not shown). The chromatogram peaks did not have a strong signal at 280 nm, and the scattering data was very broad. The addition of phosphate made data interpretation nearly impossible, and did not produce reliable data. Multiple attempts of multi-angle light scattering where performed but accurate measurements could not be made. Some additional experiments where performed at 230 nm but did not produce any signal for the chromatogram or light scattering. Furthermore, concentrating hGKA₁₂₄₋₅₅₁ to >1.0 mg/mL was unsuccessful in the SEC-MALS buffer describe above.

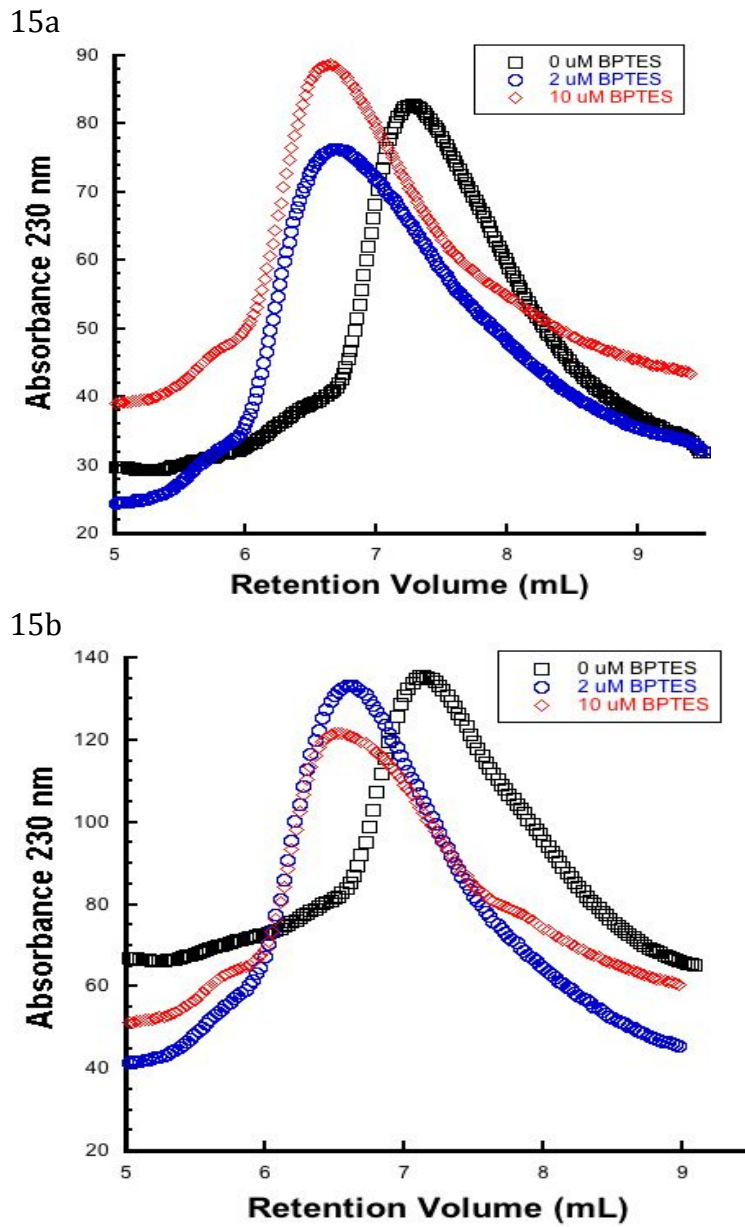


Figure 15 Gel filtration chromatography of hKGA₁₂₄₋₅₅₁
 Gel filtration chromatography was conducted by adding 80 μ L of concentrated hKGA₁₂₄₋₅₅₁ to a Bio Silect 250-5 14 mL column in 0 mM (panel A) and 100 mM phosphate (panel B) with and without the presence of BPTES. Samples were run at 0.7 mL/min and A_{230} was tracked throughout the elution. A_{230} was plotted against elution volume using KalidaGraph software. The black line represents 0 μ M BPTES while the blue and red lines represent 2 μ M and 10 μ M BPTES, respectively.

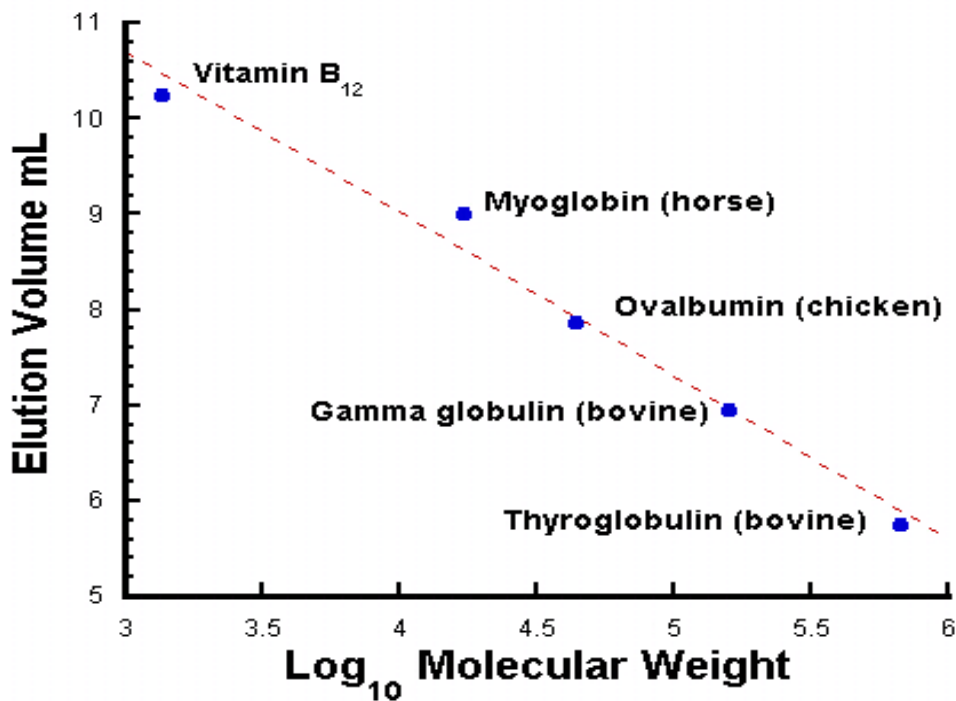


Figure 16 Gel filtration standard curve

A 50-uL sample of Bio Rad Gel Filtration Standards was injected onto a Bio-Slect 250 gel filtration column. An AKTA FPLC tracked the elution of each molecule at A_{280} nm and A_{230} nm. The peak absorbance for each molecule was used to plot the retention volume (y-axis) against the \log_{10} molecular weight (x-axis). The data were plotted using KalidaGraph software and fit to a linear curve.

Discussion

The expression protocol for hKGA₁₂₄₋₅₅₁ was performed using 2-6 L of 2xYT media. To facilitate solubility and recovery of the recombinant protein, an O.D.₆₀₀ ≥ 1.0 was achieved prior to inducing with 0.5 mM IPTG, and the temperature was lowered from 37°C to 18°C. Induction of the cell culture at 18°C with a high concentration of cells and a lower concentration of IPTG led to more cells making less target protein at a slower rate. These are distinct changes from previous expression procedures performed with a truncated form of the rat isoform of mitochondrial kidney type glutaminase (7). The expression protocol, adopted from the Structural Genomics Consortium (SGC) allowed for an apparent increase in the soluble protein fraction. However, a large portion of the target protein still resided in the pellet fraction. Sonication was the only cell disruption technique used. Using multiple sonication steps (4-6 times at high intensity) for 1 to 2 minutes, with the sample placed on ice, resulted in adequate recovery of soluble protein. Other cell disruption methods such as using a micro fluidizer were not tested to compare the efficiencies of each technique.

The purification of hKGA₁₂₄₋₅₅₁ followed the SGC protocol closely. However, it was optimized for the larger construct of human mitochondrial kidney type glutaminase that included 97 additional amino acids on the N-terminus. The IMAC purification step was very efficient and removed many contaminating proteins from the supernatant. Increasing the imidazole concentration and eluting the protein from the column in one step led to a very concentrated and cloudy solution of hKGA₁₂₄₋₅₅₁. It might have increased our protein recovery if a linear gradient of

imidazole was run during the purification to elute the hKGA₁₂₄₋₅₅₁ over a narrow range of imidazole concentrations. This could have led to the removal of more contaminants, but less protein per fraction, increasing hKGA₁₂₄₋₅₅₁ solubility. Gel filtration chromatography acted as a buffer exchange to remove the high salt concentration from the IMAC step and diluted the sample to < 1.0 mg/mL in each 3-mL fraction. These samples were very pure and remained clear for about 2 to 3 weeks at 4°C. It was found that concentrating the hKGA₁₂₄₋₅₅₁ to over 1.0 mg/mL decreased the stability of the enzyme and forced it to precipitate from solution rapidly.

The saturation data show similar results to the activities of the intact and truncated forms of the rat isoforms of KGA. The presence of DMSO does have a slight effect on the activity of the enzyme reducing the specific activity roughly 20-30% (data not shown). However, as seen with the rat isoform, the presence of BPTES in μ M concentrations had significant impact on human KGA activity. When the assay was run in 10 mM phosphate the V_{max} for the DMSO control was 8.8 ± 0.3 units/mg. In the presence of 30 mM phosphate the V_{max} for the DMSO control was 23 ± 0.4 units/mg. This suggests that phosphate still acts as a strong positive allosteric regulator of hKGA₁₂₄₋₅₅₁. Similarly, the specific activity of hKGA₁₂₄₋₅₅₁ in the presence of BPTES at 30 mM phosphate was always larger when compared to the assay performed in the presence of 10 mM phosphate. The microtiter plate assay allowed for five replicate samples at each concentration of glutamine. The data showed that maximal enzyme velocity, or V_{max} , was achieved in the presence of 20 mM glutamine. The original microtiter plate assays were performed using 0.5

mM to 80 mM glutamine range and were saturated above 20 mM glutamine. The reported data includes all glutamine data points. As seen in Supplemental Table 1, the glutamine saturation profiles in both the 10 and 30 mM phosphate solutions where curve fit differently to address the statistical significance and reproducibility and reliability of the data. The Supplemental Table shows that when each individual data point, the mean data not weighted, and the mean data weighted by its standard error generate nearly identical K_m and V_{max} values. This observation not only suggests that the modified activity assay is accurate and precise, but is reproducible. As previously mentioned, the V_{max} for hKGA₁₂₄₋₅₅₁ in the presence of BPTES decreased. Similarly, the K_m decreased as the concentration of BPTES increased. The saturation data was then plotted as Lineweaver-Burk double reciprocal plots. The transformed data sets indicated that the model of inhibition by BPTES might be mixed non-competitive at low phosphate, but is clearly uncompetitive at high phosphate concentrations. Classical non-competitive and competitive models of inhibition did not fit the current data well. At 10 mM phosphate, and low concentrations of BPTES, the inhibition data fits a mixed non-competitive model with smaller changes in K_m than V_{max} . The double reciprocal plots do not intersect the x-axis at the same point as seen in a strict non-competitive inhibition model. The linear fit of the double reciprocal plots all have a slightly different slope indicating that the intersection of the DMSO control, 0.1 μ M and 0.3 μ M BPTES occurs below the x-axis. These observations all agree with a mixed non-competitive model. On the other hand, with 30 mM phosphate, the model of inhibition fits an uncompetitive model. The saturation data transformed into double reciprocal plots

show that at each concentration of BPTES there is equivalent changes in both V_{max} and K_m . In the double reciprocal plots, the lines intersect the x-axis and y-axis at different points. Furthermore, the lines of the double reciprocal plots differ from those at 10 mM phosphate because the slopes are nearly identical for the DMSO control, 0.1 μ M, 0.3 μ M, and 0.6 μ M BPTES. The parallel behavior of the double reciprocal plots is typical of uncompetitive inhibition, where both the K_m and V_{max} change, but the slope of the line remains unchanged.

To further investigate the model of inhibition, the K_i for BPTES was calculated using both the apparent K_m and the apparent V_{max} from the glutamine saturation data at 10 mM and 30 mM phosphate. By plotting the apparent V_{max} and the apparent K_m against the concentration of BPTES, the K_i was determined. At 10 mM phosphate, the K_i values were $0.14 \pm 0.01 \mu$ M and $0.21 \pm 0.06 \mu$ M calculated from the apparent V_{max} and apparent K_m , respectively. The slight change between the K_i terms suggests the inhibition is might be mixed non-competitive. However, these changes are subtle indicating that an uncompetitive inhibition mechanism is preferred. A change in K_i will alter both the slope and intercept in a double reciprocal plot, as observed with the reported data at 10 mM phosphate and 0.1 μ M BPTES. At 30 mM phosphate, the K_i values were $0.24 \pm 0.03 \mu$ M and $0.16 \pm 0.02 \mu$ M determined from the apparent V_{max} and apparent K_m , respectively. The K_i terms are similar and correlate well with an uncompetitive model. Both the K_m and V_{max} should change in an uncompetitive inhibition model, but because the calculated K_i values were similar, the slope remains constant while the double reciprocal plots are shifted along the y-axis by the K_i inhibition term. The inhibition constant

appears to be constant for both the 10 mM and 30 mM phosphate conditions suggesting the inhibition, by BPTES, occur in an uncompetitive manner.

Phosphate is a known positive allosteric regulator of mammalian GA. As the concentration of phosphate is increased, the specific activity of hKGA₁₂₄₋₅₅₁ increased. Phosphate activation profiles were performed with a range of 5 mM to 150 mM phosphate in the presence of DMSO and BPTES. The presence of 0.5 μM BPTES lowered the specific activity of hKGA₁₂₄₋₅₅₁ by 25%, while in the presence of 10 μM BPTES the specific activity was decreased by 75% when compared to the DMSO control. From these data the $K_{0.5}$ for phosphate saturation was calculated. Increasing the concentration of BPTES in the presence of increasing phosphate concentration significantly increased the $K_{0.5}$ for phosphate suggesting a competition for binding between BPTES and phosphate. Furthermore as the concentration of BPTES was increased the Hill coefficients increased. In the DMSO control, the Hill coefficient was 1.3 ± 0.1 μM suggesting there was little cooperativity in the binding of phosphate. However, in the presence of 10 μM BPTES the Hill coefficient was 2.2 ± 0.2 μM indicating that at higher BPTES concentrations the binding of phosphate is cooperative. The graph in Figure 14 depicts this as the DMSO control has a hyperbolic curve whereas with 10 μM BPTES, the curve is sigmoidal.

To determine the molecular weight and oligomerization of hKGA₁₂₄₋₅₅₁ gel filtration chromatography and dynamic light scattering experiments were performed. It has been established that mammalian isoforms of GA oligomerize in a phosphate- dependent manner (27). Studies suggest that the inactive form of KGA exists as a dimer and the active complex of KGA is a tetramer or higher oligomer (7).

Sedimentation-velocity experiments performed in the presence of low and high phosphate showed that BPTES binds and stabilizes the tetramer form of an N-terminal truncation of rat KGA. The gel filtration data suggest the hKGA₁₂₄₋₅₅₁ behaves in a similar fashion to the rat isoform. The molecular weight of hKGA₁₂₄₋₅₅₁ is 46-kDa, as calculated from its amino acid composition. In the presence of 100 mM phosphate, and without BPTES, the predominant peak elutes from the column in a 100-kDa species indicative of a dimer. The addition of BPTES, in the presence of 100 mM phosphate, decreases the retention time. The protein now elutes from the column with a retention time equivalent to a 200-kDa species, suggesting a tetramer or higher oligomer.

Multi-angle light scattering experiments were performed in the absence and presence of BPTES at 0 mM phosphate and 150 mM phosphate. The addition of phosphate in the absence or presence of BPTES produced no results. There was a weak change in absorbance at 280 nm and no change in absorbance at 230 nm. Furthermore, there was not a strong, or any scattering signal with the addition of phosphate. However, in the absence of phosphate there was a larger change in absorbance at 280 nm in the absence and presence of BPTES. The scattering signal in the absence of phosphate was poor. These data did produce preliminary molecular weight results suggesting a dimeric, 100-kDa, form in the absence of BPTES, and a tetramer, 200-kDa, species in the presence of BPTES. However, due to the error in these measurements and the poor quality of data, these preliminary results are unreliable. Because the hKGA₁₂₄₋₅₅₁ construct was not stable in solution at concentrations higher than 1.0 mg/mL, it made multi-angle light scattering

measurements nearly impossible and very difficult to reproduce. Additional experiments where designed using less complex buffers consisting of 10 mM Tris, pH 8.0, and 150 mM KCl at 230 nm using fresh sample purified within 48 hours, but resulted in worse data collection. These findings indicated that without higher concentrations of sample, the collected data could not be reliable and different experimental techniques need to be pursued. Analytical ultra-centrifugation (AUC) studies would be more conclusive than multi-angle light scattering, and would allow accurate, reliable molecular weights of hKGA₁₂₄₋₅₅₁ homodimerization to be determined in the presence of phosphate and BPTES. Additionally, performing an intensive buffer optimization may yield conditions that allow higher concentration to be obtained. It was found that 300 mM KCl and at least 10% glycerol were essential to increasing the solubility of hKGA₁₂₄₋₅₅₁ stored at 4°C. Lower salt concentrations and the removal of glycerol from the purification or SEC-MALS buffers increased the rate of protein precipitation drastically.

The combined kinetic profiles generate a possible, yet complex model for the activation and inhibition of hKGA₁₂₄₋₅₅₁. Figure 17 describes the possible mechanisms in which hKGA₁₂₄₋₅₅₁ bind phosphate, substrate and inhibitor. In the

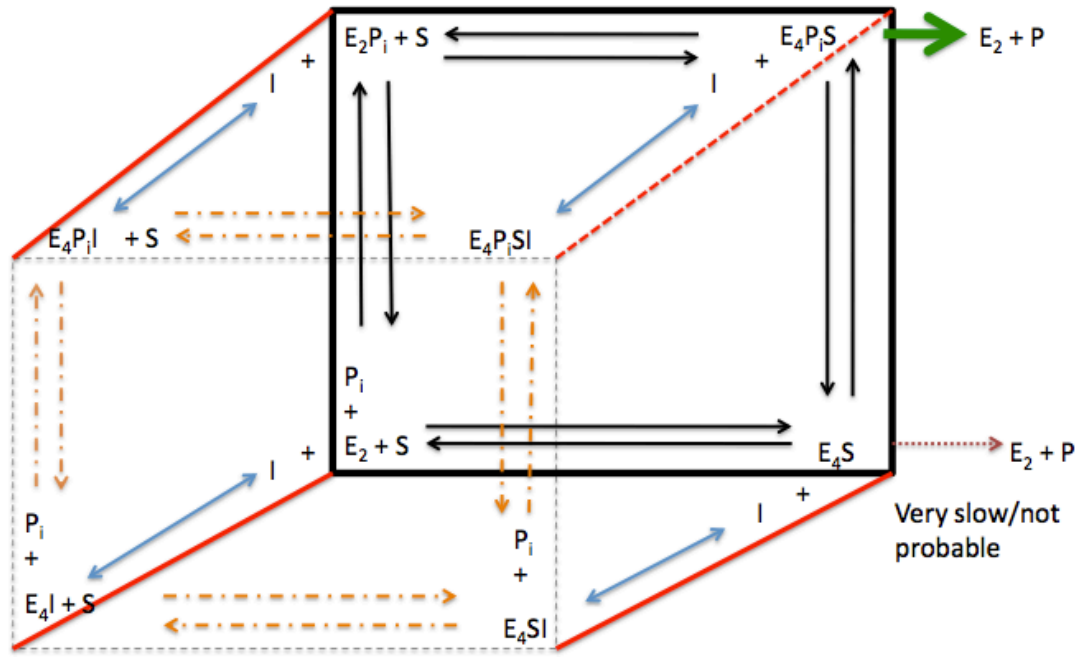


Figure 17 Proposed mechanisms of hKGA₁₂₄₋₅₅₁ in presence of phosphate and BPTES

The top (black) solid square is hKGA₁₂₄₋₅₅₁ (E) in the absence of BPTES (I). E₂ and E₄ describe the dimer and, or tetramer state the enzyme resides in. Moving from the bottom to the top of the squares is the addition of phosphate (P_i) and moving from the left of the squares to the right is the addition of glutamine, or the substrate (S). The bottom (dashed) square is enzyme in the presence of inhibitor. The solid (red) lines connecting the two squares is the addition of the inhibitor BPTES. The arrows within each of the squares suggest the possible kinetic on and off rates of each species. The small dashed arrow to the right of the cube is the small probability product is formed in the absence of phosphate and the large green arrow to the right of the cube is most probable formation of product (P).

absence of inhibitor the enzyme can bind phosphate or substrate resulting in either an enzyme substrate complex or an enzyme phosphate complex. The data indicate higher concentrations of phosphate produce larger enzymatic activities, suggesting the enzyme bound to phosphate is in an activated conformation and subsequently binds substrate in a preferred manner compared to the absence of phosphate. The enzyme-phosphate-substrate complex then performs catalysis resulting in the production of glutamine. The addition of inhibitor to this mechanism generates four additional binding possibilities; the enzyme-inhibitor complex, the enzyme-substrate-inhibitor complex, the enzyme-phosphate-inhibitor complex, and the enzyme-phosphate-substrate-inhibitor complex.

The data obtained from this study can rule out the enzyme-inhibitor complex because the inhibition data suggest the mechanism of inhibition is uncompetitive. The binding of inhibitors with free enzyme is indicative of a competitive inhibition mechanism, suggesting that the inhibitor competes with the substrate to bind the enzymatic active site. A noncompetitive inhibitor can bind either free enzyme or enzyme-substrate complex allosterically resulting in a decreased V_{max} but an unchanged K_m . The obtained data rule out this mechanism because the binding of BPTES alters both the V_{max} and K_m suggesting that it does not bind both free enzyme and enzyme-substrate complex. However, an uncompetitive inhibitor preferentially binds enzyme-substrate complex altering both V_{max} and K_m . These combined data now indicate the BPTES may preferentially bind to activated, phosphate-bound, hKGA₁₂₄₋₅₅₁ in complex with glutamine. The data further suggest, as seen in previous studies, that BPTES either binds to or forms a stable tetramer of

mammalian GA. Because the data strongly indicate an uncompetitive inhibition model, it can be proposed that BPTES only binds to enzyme-substrate complex. If this is valid, an enzyme-substrate complex is preferentially observed when hKGA₁₂₄₋₅₅₁ exists in its tetramer form in the presence of phosphate. On the other hand, the data can also suggest that BTPES alone is able to form, or induce, stable inactive tetramer complexes of hKGA₁₂₄₋₅₅₁ as seen in the gel filtration data (Figure 11). In the absence of phosphate mammalian GA, and hKGA₁₂₄₋₅₅₁ exists as a dimer, suggesting that BPTES may induce the formation of stable inactive tetramers bound to substrate. This may explain the slight cooperativity seen for phosphate at higher concentrations of BPTES.

References

1. Curthoys, N. P., and Watford, M. (1995) Regulation of glutaminase activity and glutamine metabolism, *Annu Rev Nutr* 15, 133-159.
2. Srinivasan, M., Kalousek, F., and Curthoys, N. P. (1995) In vitro characterization of the mitochondrial processing and the potential function of the 68-kDa subunit of renal glutaminase, *J Biol Chem* 270, 1185-1190.
3. Curthoys, N. P., and Weiss, R. F. (1974) Regulation of renal ammoniogenesis. Subcellular localization of rat kidney glutaminase isoenzymes, *J Biol Chem* 249, 3261-3266.
4. Curthoys, N. P., and Godfrey, S. S. (1976) Properties of rat kidney glutaminase enzymes and their role in renal ammoniogenesis, *Curr Probl Clin Biochem* 6, 346-356.
5. de la Rosa, V., Campos-Sandoval, J. A., Martin-Rufian, M., Cardona, C., Mates, J. M., Segura, J. A., Alonso, F. J., and Marquez, J. (2009) A novel glutaminase isoform in mammalian tissues, *Neurochem Int* 55, 76-84.
6. Holten, A. T., and Gundersen, V. (2008) Glutamine as a precursor for transmitter glutamate, aspartate and GABA in the cerebellum: a role for phosphate-activated glutaminase, *J Neurochem* 104, 1032-1042.
7. Robinson, M. M., McBryant, S. J., Tsukamoto, T., Rojas, C., Ferraris, D. V., Hamilton, S. K., Hansen, J. C., and Curthoys, N. P. (2007) Novel mechanism of inhibition of rat kidney-type glutaminase by bis-2-(5-phenylacetamido-1,2,4-thiadiazol-2-yl)ethyl sulfide (BPTES), *Biochem J* 406, 407-414.
8. Erickson, J. W., and Cerione, R. A. (2010) Glutaminase: a hot spot for regulation of cancer cell metabolism?, *Oncotarget* 1, 734-740.
9. Heiden, M. G. V., Cantley, L. C., and Thompson, C. B. (2009) Understanding the Warburg Effect: The Metabolic Requirements of Cell Proliferation, *Science* 324, 1029-1033.
10. Dang, C. V. (2010) Rethinking the Warburg Effect with Myc Micromanaging Glutamine Metabolism, *Cancer Research* 70, 859-862.
11. Porter, L. D., Ibrahim, H., Taylor, L., and Curthoys, N. P. (2002) Complexity and species variation of the kidney-type glutaminase gene, *Physiol Genomics* 9, 157-166.
12. Elgadi, K. M., Meguid, R. A., Qian, M., Souba, W. W., and Abcouwer, S. F. (1999) Cloning and analysis of unique human glutaminase isoforms generated by tissue-specific alternative splicing, *Physiol Genomics* 1, 51-62.
13. Kenny, J., Bao, Y., Hamm, B., Taylor, L., Toth, A., Wagers, B., and Curthoys, N. P. (2003) Bacterial expression, purification, and characterization of rat kidney-type mitochondrial glutaminase, *Protein Expr Purif* 31, 140-148.
14. DeBerardinis, R. J., and Cheng, T. (2010) Q's next: the diverse functions of glutamine in metabolism, cell biology and cancer, *Oncogene* 29, 313-324.
15. Wang, J. B., Erickson, J. W., Fuji, R., Ramachandran, S., Gao, P., Dinavahi, R., Wilson, K. F., Ambrosio, A. L. B., Dias, S. M. G., Dang, C. V., and Cerione, R. A. (2010) Targeting Mitochondrial Glutaminase Activity Inhibits Oncogenic Transformation, *Cancer Cell* 18, 207-219.

16. Deberardinis, R. J., Sayed, N., Ditsworth, D., and Thompson, C. B. (2008) Brick by brick: metabolism and tumor cell growth, *Curr Opin Genet Dev* 18, 54-61.
17. DeBerardinis, R. J., Mancuso, A., Daikhin, E., Nissim, I., Yudkoff, M., Wehrli, S., and Thompson, C. B. (2007) Beyond aerobic glycolysis: transformed cells can engage in glutamine metabolism that exceeds the requirement for protein and nucleotide synthesis, *Proc Natl Acad Sci U S A* 104, 19345-19350.
18. DeBerardinis, R. J., Lum, J. J., Hatzivassiliou, G., and Thompson, C. B. (2008) The biology of cancer: metabolic reprogramming fuels cell growth and proliferation, *Cell Metab* 7, 11-20.
19. Seltzer, M. J., Bennett, B. D., Joshi, A. D., Gao, P., Thomas, A. G., Ferraris, D. V., Tsukamoto, T., Rojas, C. J., Slusher, B. S., Rabinowitz, J. D., Dang, C. V., and Riggins, G. J. (2010) Inhibition of glutaminase preferentially slows growth of glioma cells with mutant IDH1, *Cancer Research* 70, 8981-8987.
20. Vega, F. M., and Ridley, A. J. (2008) Rho GTPases in cancer cell biology, *FEBS Lett* 582, 2093-2101.
21. Etienne-Manneville, S., and Hall, A. (2002) Rho GTPases in cell biology, *Nature* 420, 629-635.
22. Lin, R., Cerione, R. A., and Manor, D. (1999) Specific contributions of the small GTPases Rho, Rac, and Cdc42 to Dbl transformation, *J Biol Chem* 274, 23633-23641.
23. Whitehead, I. P., Campbell, S., Rossman, K. L., and Der, C. J. (1997) Dbl family proteins, *Biochim Biophys Acta* 1332, F1-23.
24. Gao, P., Tchernyshyov, I., Chang, T. C., Lee, Y. S., Kita, K., Ochi, T., Zeller, K. I., De Marzo, A. M., Van Eyk, J. E., Mendell, J. T., and Dang, C. V. (2009) c-Myc suppression of miR-23a/b enhances mitochondrial glutaminase expression and glutamine metabolism, *Nature* 458, 762-765.
25. Curthoys, N. P., Kuhlenschmidt, T., Godfrey, S. S., and Weiss, R. F. (1976) Phosphate-dependent glutaminase from rat kidney. Cause of increased activity in response to acidosis and identity with glutaminase from other tissues, *Arch Biochem Biophys* 172, 162-167.
26. Haser, W. G., Shapiro, R. A., and Curthoys, N. P. (1985) Comparison of the phosphate-dependent glutaminase obtained from rat brain and kidney, *Biochem J* 229, 399-408.
27. Morehouse, R. F., and Curthoys, N. P. (1981) Properties of rat renal phosphate-dependent glutaminase coupled to Sepharose. Evidence that dimerization is essential for activation, *Biochem J* 193, 709-716.
28. Clark, V. M., Shapiro, R. A., and Curthoys, N. P. (1982) Comparison of the hydrolysis and the covalent binding of 6-diazo-5-oxo-L-[6-14C]norleucine by rat renal phosphate-dependent glutaminase, *Arch Biochem Biophys* 213, 232-239.
29. Shapiro, R. A., Clark, V. M., and Curthoys, N. P. (1979) Inactivation of rat renal phosphate-dependent glutaminase with 6-diazo-5-oxo-L-norleucine. Evidence for interaction at the glutamine binding site, *J Biol Chem* 254, 2835-2838.

30. Holcomb, T., Taylor, L., Trohkimoisen, J., and Curthoys, N. P. (2000) Isolation, characterization and expression of a human brain mitochondrial glutaminase cDNA, *Brain Res Mol Brain Res* 76, 56-63.

APPENDIX I

Supplementary Table 1 Kinetic curve fit data set

10 mM phosphate glutamine saturation profile

All Data Fit	Apparent Km	Apparent Vmax	R Value
DMSO	1.2±0.11	8.8±0.17	0.96
0.1 µM BPTES	0.9±0.10	4.9±0.10	0.94
0.3 µM BPTES	0.6±0.09	2.7±0.07	0.84
Mean Unweighted	Apparent Km	Apparent Vmax	R Value
DMSO	1.2±0.20	8.8±0.30	0.98
0.1 µM BPTES	0.9±0.16	4.9±0.16	0.97
0.3 µM BPTES	0.6±0.16	2.7±0.13	0.91
Mean Weighted	Apparent Km	Apparent Vmax	R Value
DMSO	0.8±0.03	8.2±0.10	0.98
0.1 µM BPTES	1.1±0.06	4.9±0.07	0.98
0.3 µM BPTES	0.5±0.05	2.6±0.05	0.92
0.6 µM BPTES	0.2±0.04	1.5±0.03	0.53

30 mM phosphate glutamine saturation profile

All Data Fit	Apparent Km	Apparent Vmax	R Value
DMSO	1.5±0.10	23±0.32	0.98
0.1 µM BPTES	0.9±0.06	15±0.17	0.98
0.3 µM BPTES	0.5±0.07	9.6±0.20	0.9
0.6 µM BPTES	0.4±0.05	6.9±0.12	0.89
1.0 µM BPTES	0.2±0.05	5.3±0.12	0.68
Mean Unweighted	Apparent Km	Apparent Vmax	R Value
DMSO	1.5±0.13	23±0.43	0.99
0.1 µM BPTES	0.9±0.08	15±0.23	0.99
0.3 µM BPTES	0.5±0.04	9.6±0.13	0.99
0.6 µM BPTES	0.4±0.06	6.9±0.15	0.97
1.0 µM BPTES	0.2±0.04	5.3±0.10	0.95
Mean Weighted	Apparent Km	Apparent Vmax	R Value
DMSO	1.6±0.04	24±0.32	1
0.1 µM BPTES	0.9±0.02	15±0.16	0.99
0.3 µM BPTES	0.6±0.04	9.8±0.19	0.99
0.6 µM BPTES	0.5±0.02	7.1±0.12	0.99
1.0 µM BPTES	0.3±0.03	5.4±0.13	0.98

The specific activities, produced from the glutamine saturation profiles at 10 mM and 30 mM phosphate, were curve fit to the Michaelis-Menten equation using KalidaGraph (Synergy) software. For each concentration of phosphate the data was fit three different ways. The all data fit was the saturation data fit for each of the five replicate data points. The mean un-weighted fit was the curve fit to the mean saturation data without the standard error measurements included into the curve fit. The mean weighted fit was the mean saturation data with the standard error measurements included into the curve fit. The apparent K_m , the apparent V_{max} , and the R-values are the calculated parameters produced by the non-linear least squares fit performed by KalidaGraph for each curve fit.